frontiers | Frontiers in Energy Research

TYPE Review
PUBLISHED 17 January 2023
DOI 10.3389/fenrg.2022.1029477

OPEN ACCESS

EDITED BY
Uwe Schröder,
University of Greifswald, Germany

REVIEWED BY
Srirat Chuayboon,
King Mongkut's Institute of Technology Ladkrabang, Thailand
Pedro Haro,
Universidad de Sevilla, Spain

*CORRESPONDENCE
Yanjun Dai,
yjdai@sjtu.edu.cn

SPECIALTY SECTION
This article was submitted to Solar Energy, a section of the journal Frontiers in Energy Research

RECEIVED 27 August 2022
ACCEPTED 08 November 2022
PUBLISHED 17 January 2023

CITATION
Xu D, Gu X and Dai Y (2023), Concentrating solar assisted biomass-to-fuel conversion through gasification: A review.
Front. Energy Res. 10:1029477.
doi: 10.3389/fenrg.2022.1029477

Concentrating solar assisted biomass-to-fuel conversion through gasification: A review

Dequan Xu[1,2], Xinzhuang Gu[1,2] and Yanjun Dai[1,2]*

[1]Institute of Refrigeration and Cryogenics, Shanghai Jiao Tong University, Shanghai, China, [2]Engineering Research Center of Solar Energy and Refrigeration, MOE, China

Solar energy, the most abundant and exploitable renewable energy resource, is regarded as a major energy source for the future. Nevertheless, solar irradiation is characterized by relatively low energy density, intermittency and uneven distribution. Storage of solar energy for usage during non-solar times is required to match supply and demand rates in today's society. In this context, the application of solar energy for converting into storable, transportable, and energy-dense fuels (i.e., solar fuels) is an attractive option, with the advantage of contributing to promoting the commercialization of solar power technologies. Solar assisted biomass gasification is a promising pathway to produce solar fuels. With concentrated solar energy providing reaction heat, carbonaceous materials can be converted to high grade syngas, which could be further synthesized into useful hydrocarbon fuels. In such process, solar energy is stored in a chemical form, with solar spectrum fully utilized. Compared with autothermal biomass gasification, the usage of high-flux concentrated solar radiation to drive endothermic gasification reactions improves energy efficiencies, saves biomass feedstocks, and is relatively free of combustion by-products. This review presents a comprehensive summary of solar assisted biomass gasification, including concentrating solar technology, fundamentals of solar biomass gasification, state-of-the-art solar gasifier designs, strategies for solar intermittence management, and downstream applications.

KEYWORDS

concentrated solar, biomass gasification, solar fuel, syngas, intermittence management

1 Introduction

As concerns increase worldwide regarding the rapid depletion of fossil fuels, the resulting greenhouse gas emissions and global warming, renewable energy sources have attracted more and more attention for gradually replacing fossil fuels (Fukuzumi, 2017; Cao et al., 2020). Solar energy is by far the largest renewable energy source exploitable - Continuous solar radiation reaches the Earth at a rate of 173,000 TW. Nevertheless, solar irradiation is characterized by relatively low energy density, intermittency and uneven distribution (Loutzenhiser and Muroyama, 2017). In order to match the energy demand of today's society, solar energy needs to be stored for usage during off-solar periods. The conversion of solar radiation into

storable, transportable, and energy-dense fuels (i.e., solar fuels) is an attractive option that could help to promote the commercialization of solar power technologies (Shih et al., 2018; Bayon et al., 2020; Troiano et al., 2022).

As shown in Figure 1, the utilization of concentrated solar energy to propel thermochemical conversions is one potential route for the production of solar fuels (Steinfeld, 2005). According to different types of reactants, the technique map can be divided into non-carbonaceous routes and carbonaceous routes. Non-carbonaceous routes involve solar splitting H_2O and CO_2 through direct thermolysis or multi-step thermochemical cycles, producing combustible gases H_2 and CO. As direct thermolysis is a strongly endothermic reaction, an extremely high temperature is needed (usually >2,200°C), resulting in stricter operation conditions and inevitable irreversible loss in the product separation process. Multistep thermochemical cycles can automatically separate the product and greatly lower the reaction temperature, among which the two-step thermochemical cycle is the most favored for its simplicity (Centi and Perathoner, 2010; Roy et al., 2010). Numerous studies had focused on the ideal layout of the solar receiver-reactor (Agrafiotis et al., 2015; Chuayboon and Abanades, 2020; Wang et al., 2022) and the development of new catalysts (Bayon et al., 2020). Despite being hopeful, the conversion efficiency of solar splitting of H_2O and CO_2 remains a significant obstacle (Schappi et al., 2021). Additionally, carbonaceous routes can be taken by using methane (Li Z. et al., 2020), biomass or coal as feedstocks. The production of syngas (H_2 and CO) can be achieved from solar thermochemical gasification, cracking or reforming processes, and it could be further synthesized into useful hydrocarbon fuels by Fischer-Tropsch synthesis (FTS). With water-gas shift (WGS) reaction or carbon capture and sequestration applied, solar hydrogen can be produced from any of these processes as well.

Because of its renewability and diversity as an energy source, biomass is gaining popularity. Energy crops and crop leftovers, wood and wood wastes, agricultural wastes, grass, residential waste, animal and municipal wastes, aquatic plants, food processing waste, and algae are all examples of biomass feedstocks (Baruah et al., 2018). The technologies applied to generate power from biomass include combustion, thermochemical, and biochemical conversions (Tanger et al., 2013; Kaur et al., 2019). Gasification and pyrolysis are the two primary thermochemical conversion pathways for biomass (Wang et al., 2017). It is believed that biomass gasification is a more efficient method of producing syngas than pyrolysis as it operates at a higher temperature and in the presence of an oxidizing agent (Cao et al., 2020). Syngas can be used to generate electricity, heat, and produce synthetic chemicals such as methanol, dimethyl ether, and ammonia. Furthermore, hydrogen of high purity derived from additional CO conversion in syngas may be utilized in fuel cells (Fukuzumi, 2017). Power generation from gasification products enables a 10x reduction in SO_2 and NOx emissions as compared to direct burning of biomass feedstocks (Basu, 2010), since it is easier to remove pollutants from a syngas stream than to clean the flue gas emitted from direct biomass combustion.

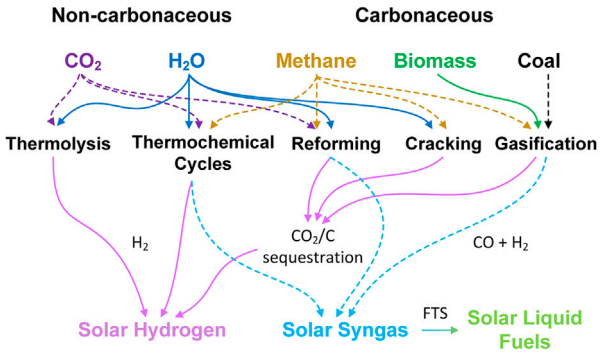

FIGURE 1
A technique map of thermochemical solar fuel production. Reproduced from (Bayon et al., 2020).

Conventional autothermal biomass gasification (Yoon et al., 2011; Li et al., 2021c) necessitates burning a portion of the feedstock to induce highly endothermic processes, reducing the total energy content of the outputs (Heidenreich and Foscolo, 2015). A solar-biomass combination is a prospective way to compensate for inadequacies (Li and Wang, 2020). Solar infrastructures such as solar towers and parabolic dishes can concentrate solar irradiation above 1,000 suns (1 Sun = 1 kW m^{-2}), making them ideal for driving any high-temperature solar thermochemical process. With concentrated solar energy providing reaction heat, carbonaceous materials can be converted to high grade syngas, which could be further synthesized into useful hydrocarbon fuels (Chu and Majumdar, 2012). In such process, solar energy is stored in a chemical form, with solar spectrum fully utilized (Figure 2). The biomass feedstock is also converted into a fuel that has a wider variety of versatile uses. In addition to solar reactor-based gasification, some other solar biorefinery processes are also valued for converting biomass into a spectrum of marketable products and energy (Golberg et al., 2021; Gutiérrez et al., 2022; Karan et al., 2022).

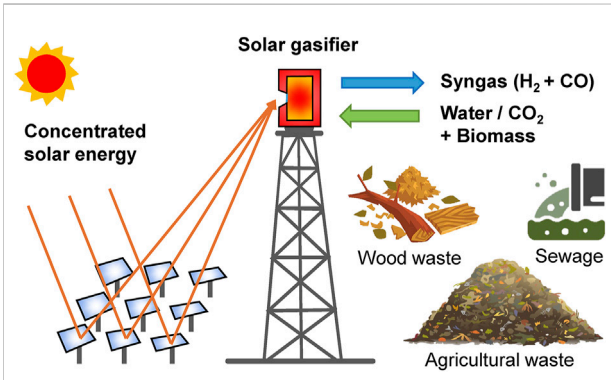

FIGURE 2
Schematic of solar gasification with biomass feedstocks.

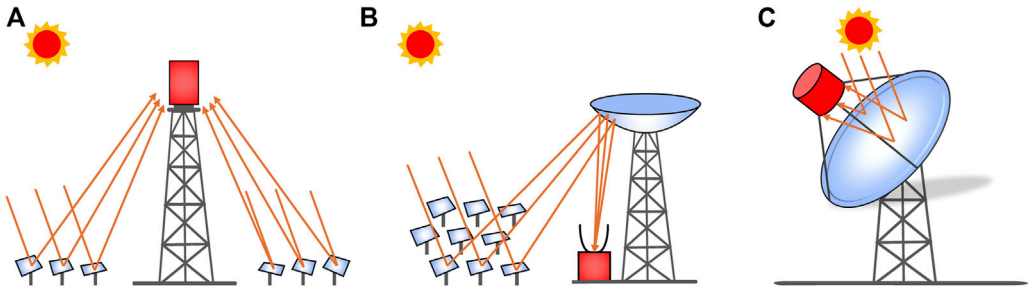

FIGURE 3
Schematics of point-focusing solar concentrating technologies: **(A)** a traditional solar tower system, **(B)** a beam-down concentrating solar tower, and **(C)** a parabolic dish.

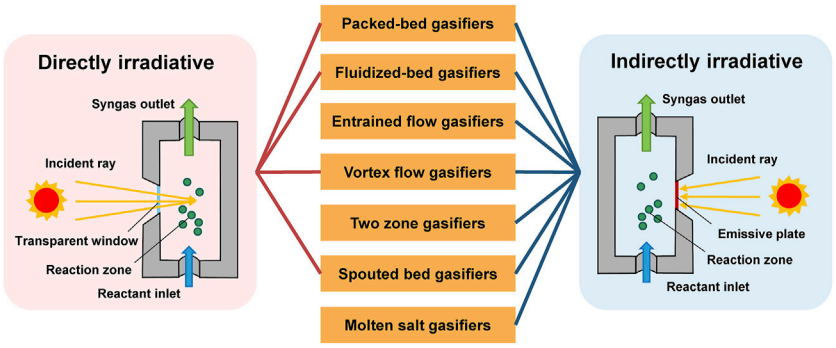

FIGURE 4
Different categories of solar gasifiers for biomass gasification.

(Piatkowski et al., 2011) summarized fundamental thermodynamics and kinetics for solar-driven biomass gasification. Some preceding solar gasifier designs for biomass gasification were reviewed by (Puig-Arnavat et al., 2013; Loutzenhiser and Muroyama, 2017). Most recently, (Jie Ling et al., 2022), discussed several hybrid solar-biomass thermo-chemical conversion systems. (Fang et al., 2021) concluded concentrated solar thermochemical gasification of biomass (CSTGB) from a whole system perspective. (Abanades et al., 2021) reviewed solar reactor concepts and modeling methods for biomass pyro-gasification, especially on spouted bed reactors. This review aims to present a comprehensive summary of solar assisted biomass gasification: Section 2 introduces concentrating solar technology; Section 3 presents the working principle of solar biomass gasification technology; Section 4 shows the main approaches to manage solar intermittence; Section 5 depicts different utilization forms of synthesis gas. Finally, the future prospects and conclusions are summarized in Section 6 and Section 7, respectively.

2 Concentrated solar energy

The Sun, with a solar radiosity of 63 MW/m^2, is an infinite supply of thermal energy comparable to a 5800 K blackbody at origin, offering the most plentiful and accessible renewable energy source. The direct normal incident solar radiation (DNI) distributed on the Earth's surface, however, may scarcely reach 1000 W/m^2 since the Sun's rays come in a diluted form. Specialized solar equipment must be employed to capture solar irradiation and transform it into heat or chemical energy. Solar concentrators facilitate energy delivery at high temperatures, making them essential in a wide range of engineering applications. High flux can be achieved with only modest thermal losses thanks to optical concentration devices. They are made up of broad reflecting surfaces that gather solar radiation as it strikes them and focus it onto a solar receiver.

TABLE 1 Key information on solar tower facilities used for solar thermochemical processes. (Villafán-Vidales et al., 2017).

No.	Solar tower	Country	Tower description	Thermochemical process	References
1	Weizmann Institute of Science Solar Tower	Israel	Beam-down configuration	CO_2 reforming of methane	Wörner and Tamme, (1998)
			A hyperbolic 75 m^2 reflector	Steam reforming of methane	Möller, (2008)
			45 m above ground level	Carbothermic reduction of ZnO	Wieckert et al. (2006)
			Nominal power: 1 MW		
2	SSPS-CRS at Plataforma Solar de Almería	Spain	A north field with 91 heliostats	Two-step water splitting	Roeb et al. (2011)
			A 43 m tower		
			Nominal power: 2.5 MW		
3	CESA-1 Tower at Plataforma Solar de Almería	Spain	A north heliostat field	Gasification of carbonaceous materials	Wieckert et al. (2013)
			An 80 m high concrete tower		
			Nominal power: 5 MW		
4	CSIRO Solar Tower 1	Australia	An 804 m^2 reflector area	Steam reforming of natural gas	Agrafiotis et al. (2014)
			Consist of 179 heliostats		
			Nominal power: 0.5 MW		

2.1 Solar concentrators

Solar concentrators follow the basic optical law for reflection by specular surfaces. From an energetic point of view, their concentration capability is expressed by flux concentration ratio C_f defined as the area-mean radiative power flux incident at the focused receiver area, normalized to the DNI.

$$C_f = \frac{\dot{Q}_{rec}}{DNI \cdot A_{rec}} \tag{1}$$

Given the fact that the flux on the focused area is non-uniformly distributed and hard to measure, geometrical concentration C_g is introduced for convenience. It is described as the proportion of the aperture areas of the concentrator and receiver, A_{conc} and A_{rec}, respectively.

$$C_g = \frac{A_{conc}}{A_{rec}} \tag{2}$$

In practice, the concentration ratio is constrained by the restricted divergence angle of sunlight on Earth. The concentrator's rim angle ψ_{rim} and the principle of etendue conservation are used to calculate the highest concentration ratio C_{max} that can be achieved (Weinstein et al., 2015):

$$C_{g,max,2D} = \frac{\sin \psi_{rim}}{\sin \theta_{sun}} \tag{3}$$

$$C_{g,max,3D} = \left(\frac{\sin \psi_{rim}}{\sin \theta_{sun}}\right)^2 \tag{4}$$

where $C_{g,max,2D}$ and $C_{g,max,3D}$ are the maximum geometrical concentration ratios for two-dimensional (line-focusing) and three-dimensional (point-focusing) systems, respectively. θ_{sun} is half of the divergence angle of sunlight on Earth (4.8 mrad). The rim angle ψ_{rim} is the greatest angle at which the concentrator's reflected light hits the receiver. When the rim angle reaches a maximum of 90°, the highest achievable concentration ratio for a 2-D system is roughly 208 and 43,400 for a 3-D system. Due to imprecise tracking and defects in reflector surfaces, real concentrators cannot attain such high concentration ratios (Weinstein et al., 2015).

Parabolic concentrators and their analogues are commonly applied in industry. Because of their greater concentration ratios, 3-D point-focusing concentrators are more practicable for driving solar gasification, as the gasification process requires the operation temperature normally >800°C. Typical types of point-focusing solar concentrator are depicted in Figure 3. The traditional solar tower configuration (Figure 3A, also called a central receiver system) is a three-dimensional concentrating system that directs incident solar rays to a solar receiver installed on top of a tower. Typically, C ranges from 300 to 1,500, and the operating temperature can reach over 1,000°C. Another point-focusing concentrator is the parabolic dish (Figure 3C), and its concentration ratio may easily exceed 1,000 at the tradeoff of more complexity and expense. Since parabolic dishes are restricted in size, for large-scale thermal applications the solar tower system is the most desirable approach.

2.2 Solar tower system

As mentioned above, the solar tower system is becoming more appealing and exhibits a great potential for coupling with large-scale, high-temperature thermochemical processes (Weinstein et al., 2015). In a solar tower system, the solar

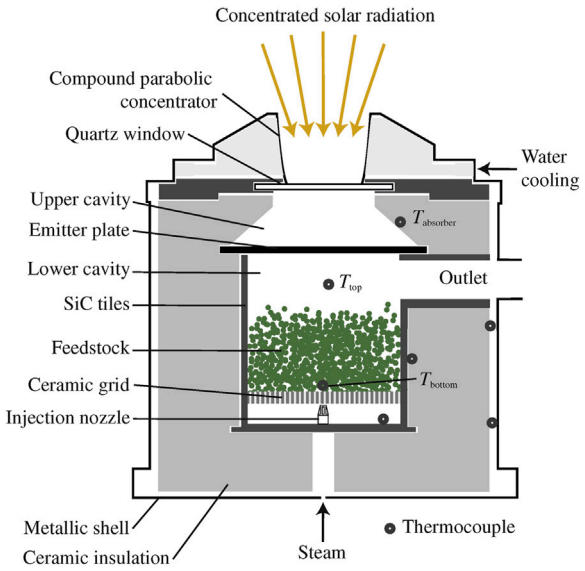

FIGURE 5
Schematic of the solar packed-bed reactor. Reproduced from (Müller et al., 2018).

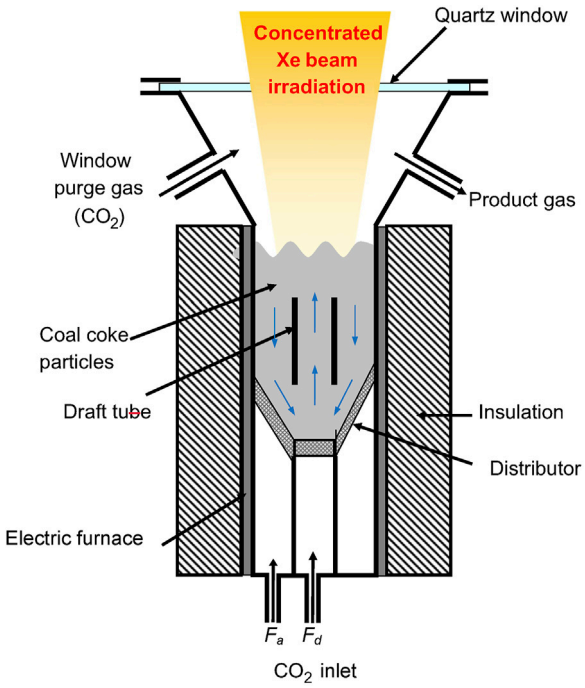

FIGURE 6
An internally circulating fluidized bed reactor coupled with beam down optical layout. Adapted from (Gokon et al., 2012).

field consists of numerous auto-controlled mirrors (heliostats) that track the Sun individually in two axes and reflect the direct solar radiation onto the central receiver (CR) located on the tower. The CR absorbs reflected solar radiation and converts it into thermal energy. To ensure a high optical efficiency, especially in scaled-up plants, a tower of ~100 m above the ground is required. The challenges that brought by a tall tower include the increase in the maintenance difficulty of the receiver and significant heat loss and pump power requirement in heat transport from the solar receiver to power subsystem (Li et al., 2017). To make up for the deficiencies, a beam-down concentrating solar tower has been proposed and developed as a promising alternative technology (Rabl, 1976). Beam down layout utilizes a Cassegrain optical setup that was adapted from telescopes. As shown in Figure 3B, a secondary hyperboloid or ellipsoid reflector at the top of the tower directs the light impinging on it in the direction of the cavity receiver, which is placed on the ground (Li et al., 2015). The tower's weight and cost are greatly reduced as a result as it now only supports the secondary reflecting component (Yogev et al., 1998). On the other hand, beam-down concept has some issues, which have been pointed out by (Vant-Hull, 2014).

The overall optical efficiency of a solar tower system, η_{opt}, is defined as the ratio of power captured by the receiver aperture $\dot{Q}_{rec}$ to the maximum potential power that could be received by the entire heliostat field (Lipiński et al., 2021). The maximum possible radiant power that can be collected is calculated when solar rays are normally incident on the total installed area of the mirrors in the heliostat field A_{conc}.

$$\eta_{opt} = \frac{\dot{Q}_{rec}}{DNI \cdot A_{conc}} \quad (5)$$

Therefore, Eq. 5 is a measure of how efficiently the heliostat field transfers solar radiation to the central receiver. As the heliostat field generally accounts for 30–50% of the capital cost of a solar tower system, improving the optical performance of the optical sub-system is essential for cost reduction (Li et al., 2016).

2.2.1 Heliostat field

There are cosine losses, reflection losses, shadowing and blocking losses, atmospheric attenuation losses and spillage losses in the process of receiving and reflecting sunlight by heliostats. For this reason, when arranging the heliostat array, the causes of these losses should be avoided appropriately, so that more solar radiation energy can be collected. 1) Cosine loss. In order to reflect solar energy to a fixed target, the surface of the heliostat cannot always remain perpendicular to the incident light, and may be at a certain angle. Cosine loss is due to this tilt caused by the heliostat surface area relative to the sunlight visible area reduction and produced. 2) Reflection loss. The reflection loss is caused by the reflectivity of the heliostat mirror surfaces being less than 1. 3) Shadowing and blocking losses. Shadowing loss occurs when the reflective surface of the heliostat is in the shadow of one or more adjacent heliostats, and thus cannot

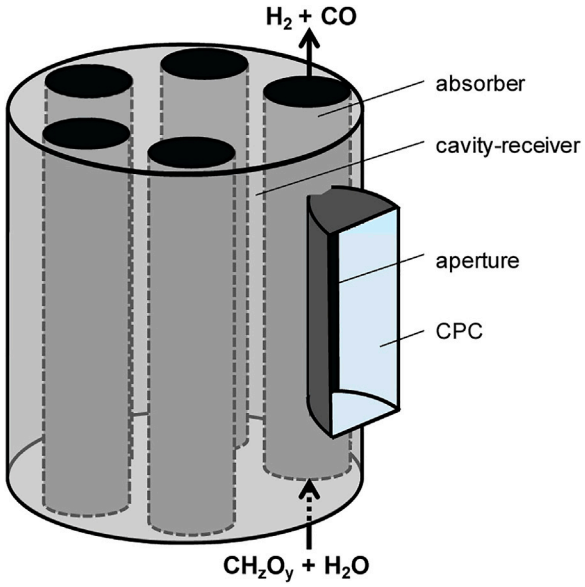

FIGURE 7
A schematic diagram of an entrained flow gasifier. Reproduced from (Maag and Steinfeld, 2010).

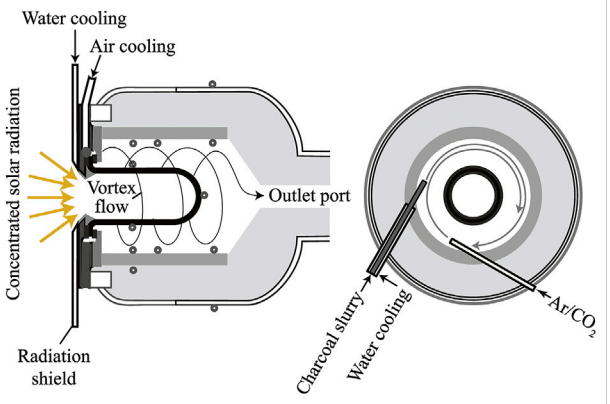

FIGURE 8
A schematic diagram of a vortex flow gasifier. Reproduced from (Müller et al., 2017).

receive solar radiation energy, this situation is particularly serious when the Sun is at a low altitude. The shading of receiving towers or other objects may also cause some shadow loss to the heliostat array. When the heliostat is not in the shadow area, the blocking loss is resulted from the reflected solar radiation blocked by the back of the adjacent heliostats, causing the solar radiation cannot reach the receiver. 4) Attenuation loss. The solar radiation energy in the atmospheric propagation process of attenuation caused by the energy loss is called attenuation loss. The degree of attenuation is usually related to the location of the Sun, the local altitude and the rate of change in absorption due to atmospheric conditions. 5) Spillage loss. The solar radiation energy reflected from the heliostat does not reach the surface of the absorber and spill into the outside atmosphere, resulting in energy loss is called spillage loss. In view of this, the product of each efficiency element can be used to represent the overall optical efficiency.

$$\eta_{opt} = \eta_{cosine}\,\eta_{reflection}\,\eta_{shadow}\,\eta_{block}\,\eta_{attenuation}\,\eta_{spillage} \quad (6)$$

A representative value of overall optical efficiency is approximately 67.45% annually for the Planta Solar 10 (PS10) solar power plant (10MW, in Andalusia, Spain), broken down into 84.40%, 88.00%, 96.56%, 99.09%, 95.50%, and 99.39% for cosine, reflection, shading, blocking, attenuation and spillage efficiencies, respectively (Rinaldi et al., 2014). A detailed review of state of the art in design of heliostats was presented by (Pfahl et al., 2017).

2.2.2 Solar receiver

Solar receiver is the key component in high-temperature solar energy utilization, which directly converts the solar energy captured, reflected and concentrated by the heliostat into high-temperature thermal energy that can be utilized efficiently. There are two design alternatives based on geometrical configuration: external and cavity-type receivers. The external receiver can receive radiation all around the circumference, which is conducive to the layout design of the heliostat field and the large-scale utilization of solar energy. However, since the heat absorber is exposed in the surrounding environment, a large heat loss is observed, and the receiver thermal efficiency is relatively low at high temperatures. For a cavity receiver, the aperture solely receives fluxes from one side of the solar tower. The fraction of incident radiation absorbed by the cavity-type receiver far surpasses the surface absorptance of the inner wall due to internal reflections. With the ratio of the cavity's characteristic length to the aperture diameter increasing, the cavity receiver becomes close to a blackbody absorber (Romero and Steinfeld, 2012). The absorption efficiency may be expressed as follows for an assuming isothermal and completely insulated blackbody cavity-receiver with no heat losses through reflection, conduction, or convection:

$$\eta_{abs} = 1 - \frac{\sigma T_{rec}^4}{\mathrm{DNI} \cdot C_f} = 1 - \frac{\sigma T_{rec}^4}{\eta_{opt} \cdot \mathrm{DNI} \cdot C_g} \quad (7)$$

Reduced radiative heat losses from a smaller receiver aperture are possible with high concentration ratios. This encourages the development of high-concentration-ratio solar concentrators (Li L. et al., 2021). Usually, solar receiver is also a solar reactor in solar thermochemical gasification. Thus, special designs are needed considering mass and heat transfer, together with heterogeneous chemical reactions. Cavity receiver-reactors are often adopted in

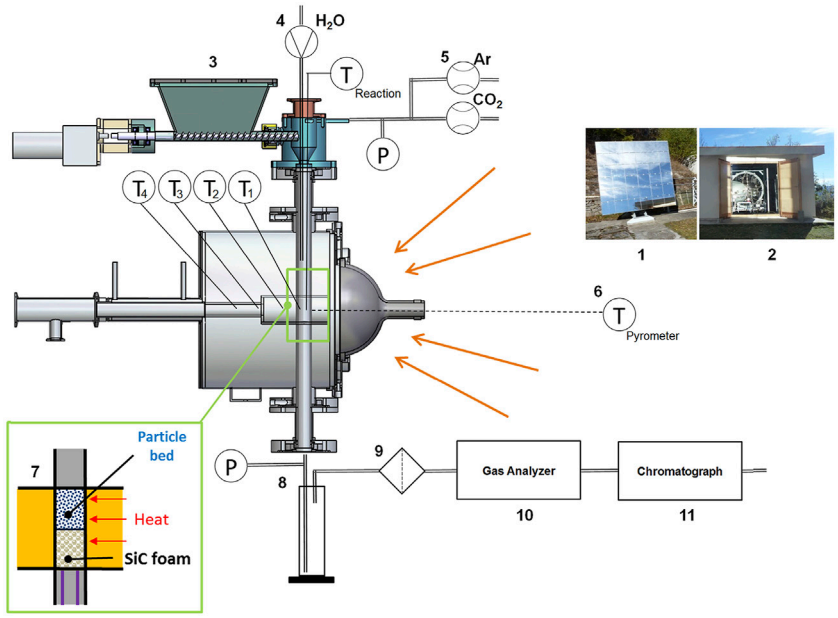

FIGURE 9
A schematic diagram of a combined drop-tube and packed-bed gasifier. Reproduced from (Bellouard et al., 2017b).

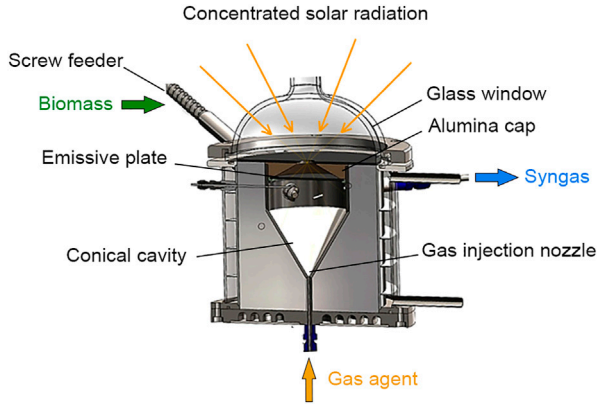

FIGURE 10
Solar conical spouted bed reactor. Adapted from (Bellouard et al., 2019).

high-temperature solar-driven biomass gasification reactions. The detailed information on solar gasifier designs and their performance indicators will be included in Section 3.

2.2.3 Solar towers for thermochemical processes

Solar tower technology was originally conceived for electricity generation (He et al., 2020); however, it is now regarded as the optimal option to conduct solar thermochemical processes at a large scale (Villafán-Vidales et al., 2017). Some papers on experimental applications of solar thermochemical processes in real solar towers have been published, verifying the feasibility of such technology. Key information of some of these facilities is summarized in Table 1. It is worth noting that the facilities in Table 1 are for a reduced scale, and their maturation has not yet reached a point that permits their adoption on a broader scale. The commercial application of such technology necessitates resolving issues in fundamental research and technological development. In the following sections, solar thermochemical processes based on biomass gasification will be specifically discussed.

3 Solar biomass gasification

3.1 Overview

A potential method for converting biomass into high-quality syngas, i.e., a combination of mostly CO and H_2, while reducing undesired byproducts, is solar-driven pyrolysis and gasification. Both pyrolysis (Zhou et al., 2018) and gasification are endothermic processes that store heat chemically to produce solid carbon, char and synthesis gas with high calorific value. According to (Arribas et al., 2017), gasification generates a larger percentage of syngas in total product gas than pyrolysis. The proportion of syngas generated *via* pyrolysis and gasification ranged 63–74% and 82–90%, respectively.

In studies of biomass gasification, steam and CO_2 are the most favorable gas agent for many researchers. Pyrolysis and

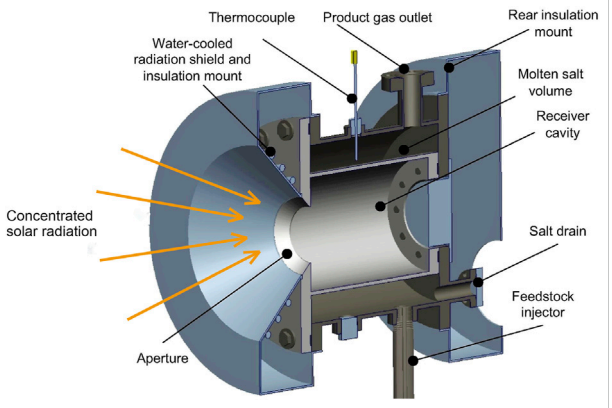

FIGURE 11
Schematic of the molten salt solar gasification reactor. Adapted from (Hathaway and Davidson, 2017).

char gasification are the two chemical processes that are primarily involved in the CO_2 or steam gasification of carbonaceous feedstocks. For stoichiometric carbon dioxide or water delivery, the whole net reaction can be expressed as

$$CH_xO_y + (1-y)CO_2 \rightarrow (2-y)CO + \frac{x}{2}H_2 \ \Delta H > 0 \quad (8)$$

$$CH_xO_y + (1-y)H_2O \rightarrow CO + \left(1 + \frac{x}{2} - y\right)H_2 \ \Delta H > 0 \quad (9)$$

where x and y represent the feedstock's H/C and O/C elemental molar ratios, respectively. For simplicity, other minor elements such as N and S are neglected in the formula. Intermediate reactions in this thermochemical process are shown as follows (Piatkowski et al., 2011; Bai et al., 2018; Jie Ling et al., 2022).

Pyrolysis:

$$\text{Biomass} \rightarrow C_{(s)} + CO + CO_2 + H_2 + CH_4 + \text{tars} \quad (10)$$

Gasification of char:

$$C + H_2O \rightarrow CO + H_2 \qquad \Delta H_1 = 131.29\text{kJ/mol} \quad (11)$$

$$C + 2H_2O \rightarrow CO_2 + 2H_2 \qquad \Delta H_2 = 90.12\text{kJ/mol} \quad (12)$$

Boudouard reaction:

$$C + CO_2 \rightarrow 2CO \qquad \Delta H_3 = 172.46\text{kJ/mol} \quad (13)$$

Methanation:

$$C + 2H_2 \rightarrow CH_4 \qquad \Delta H = -74.81\text{kJ/mol} \quad (14)$$

Steam methane reforming:

$$CH_4 + H_2O \rightarrow CO + 3H_2 \qquad \Delta H = 206.10\text{kJ/mol} \quad (15)$$

Water-gas shift (WGS):

$$CO + H_2O \rightarrow CO_2 + H_2 \qquad \Delta H = -41.17\text{kJ/mol} \quad (16)$$

The detailed process is composed of three major reaction steps (Abanades et al., 2021). The first one is the pyrolysis occurring typically in the temperature range 300–1,000°C, where biomass is thermally decomposed into incondensable gases, chars, and tars. Following pyrolysis, char acts as a reactant in the highly endothermic gasification process with injection of an oxidizing agent in the second step. Different gas phase reactions, such as the reforming and Boudouard reactions, occur in a third stage. The Boudouard reaction, Eq. 13, becomes important for CO_2-based gasification at above 1000 K. The WGS reaction, Eq. 16, which permits modifying the syngas composition for catalytic reforming to liquid fuels, is of special interest. At high temperatures, the WGS equilibrium shifts to the reactants and is hence carried out with additional catalysts at low temperatures (Piatkowski et al., 2011).

The traditional approach for supplying heat required in endothermic reactions is partial combustion of at least 30% of biomass feedstock (autothermal gasification). Inevitably, the resulting syngas has a lower calorific value, a higher CO_2 concentration, and a lower H_2/CO ratio due to such combustion. On the contrary, the heat needed for the gasification process is provided by solar radiation in a hybridized solar-biomass system. Consequently, the system showed an overall increase in the H_2/CO ratio and a decrease in the CO_2/CO ratio (Kruesi et al., 2013).

As concluded by (Müller et al., 2017), several factors make the solar-driven approach superior to the traditional autothermal process. First, it produces more synthesis gas per unit of feedstock since no feedstock is burned to provide reaction heat. Second, it generates syngas with a greater calorific value and lower CO_2 intensity with the feedstock's energy content being upgraded by solar energy input. Third, it enables higher reaction temperatures, leading in quicker reaction kinetics and fewer byproducts. Fourth, it does away with the requirement for upstream air separation during oxy-combustion. At last, solar gasification provides a productive way to store sporadic solar energy in a dispatchable and transportable chemical form (Piatkowski et al., 2011).

3.2 Performance metrics

The key performance metrics for solar biomass gasification are carbon conversion rate X_C, energy upgrade factor U (also called cold gas efficiency) and solar-to-fuel energy conversion efficiency $\eta_{\text{solar-to-fuel}}$. The carbon conversion rate, X_C, represents the percentage of the initial carbon mass in the biomass feedstock that has been converted:

$$X_C = 1 - \frac{m_{C,\text{residue}}}{m_{C,\text{feedstock}}} \quad (17)$$

X_C less than one is caused by unconverted char and particle entrainment (Curcio et al., 2021). Another more favored way to examine carbon conversion rate is to measure the percentage of

TABLE 2 Comparison of experimental performance of the most important reactor designs for solar gasification of carbonaceous feedstock (Puig-Arnavat et al., 2013).

References	Reactor type	Reactor scale (kW)	Irradiated mode	Operation mode	Gasification agent	Feedstock	Performance metrics			
							X_c	U	$\eta_{solar-to-fuel}$	$\eta_{solar-to-chem}$
Piatkowski et al. (2009)	Packed-bed	5	Indirectly	Batch	Steam	Industrial sludge	0.77	1.07	28%[c]	
						Sewage sludge	0.61	1.16	18%[c]	
						Scrap tire powder	0.91	0.83	17.3%[c]	
						Fluff	1.00	0.69	15.9%[c]	
						South African coal	0.56	1.25	23.3%[c]	
						Beech charcoal	0.87	1.30	29%[c]	
Wieckert et al. (2013)	Packed-bed	150	Indirectly	Batch	Steam	Low-rank coal	0.57	1.26	35%[c]	
						Tire chips	0.70	1.07	27%[c]	
						Fluff	0.99	1.03	25%[c]	
						Dried sewage sludge	1.00	1.05	22%[c]	
						Industrial sludge	0.36	1.14	25%[c]	
						Sugar cane bagasse	0.92	1.30	27%[c]	
Müller et al. (2018)	Packed-bed	5	Indirectly	Batch	Steam	Cotton boll	1.00	1.02	15.0%	
						Soybean husk	1.00	1.06	17.9%	
						Husk and straw	1.00	1.04	13.3%	
Kodama et al. (2002)	Fluidized-bed		Directly	Batch	CO_2	Bituminous coal	0.40			8%
Kodama et al. (2010)	Fluidized-bed	1.1	Directly	Batch	CO_2	Coal coke	0.42			14%
Gokon et al. (2012)	Fluidized-bed	3	Directly	Batch	CO_2	Coal coke	0.73			12%
Gokon et al. (2014)	Fluidized-bed	3.2	Directly	Batch	Steam	Coal coke	0.60–0.95			5–13%
Gokon et al. (2015)	Fluidized-bed	3.2	Directly	Batch	Steam	Coal coke	0.43–0.63			5.5–9.7%
Muroyama et al. (2018)	Fluidized-bed	1.5	Indirectly	Continuous	Steam	Lignite coal	0.67	1.13	16.0%[c]	
						Activated charcoal	0.74	1.11	22.1%[c]	
					Steam + O_2[a]	Activated charcoal	0.79	0.74	15.4%[c]	
Gokon et al. (2019)	Fluidized-bed	5	Directly	Batch	Steam	Coal coke	0.42–0.99			1.1–13.2%
Li et al. (2021b)	Fluidized-bed	7	Indirectly	Batch	CO_2	Charcoal	0.53	0.883	5.3 ± 0.6%[b]	
Melchior et al. (2009)	Entrained flow	3	Indirectly	Continuous	Steam	Beech charcoal	0.25			1.53%[b]
Z'Graggen et al. (2006)	Vortex flow	5	Directly	Continuous	Steam	Petcoke	0.87			4.8–8.6%
Z'Graggen et al. (2007)	Vortex flow	5	Directly	Continuous	Steam	Petcoke–water slurry	0.87			0.5–4.7%
Z'Graggen et al. (2008)	Vortex flow	5	Directly	Continuous	Steam	Petroleum vacuum residue	0.16–0.50		7.3–19.0%[b]	0.8–2.0%
Müller et al. (2017)	Vortex flow	3	Indirectly	Continuous	Steam	Charcoal-water slurry	0.78	1.18	19.7%[c]	
Kruesi et al. (2014)	Two-zone	1.5	Indirectly	Continuous	Steam	Sugarcane bagasse	0.90	1.06	21.6%[c]	
Bellouard et al. (2017b)	Two-zone	1	Indirectly	Continuous	Steam	Wood	0.94	1.21	28%	
						Torrefied wood	0.81	1.02	18.3%	
Dai et al. (2022)	Two-zone	1.5	Indirectly	Continuous	Steam	Lignite Coal	0.50–0.70	1.14–1.17	20–24%[c]	
Bellouard et al. (2019)	Spouted bed	1.5	Indirectly	Continuous	Steam	Beech wood	0.95	1.21	15.6–30.9%	
					CO_2		0.82	1.09	25.8%	

(Continued on following page)

TABLE 2 (*Continued*) Comparison of experimental performance of the most important reactor designs for solar gasification of carbonaceous feedstock (Puig-Arnavat et al., 2013).

References	Reactor type	Reactor scale (kW)	Irradiated mode	Operation mode	Gasification agent	Feedstock	Performance metrics			
							X_c	U	$\eta_{solar-to-fuel}$	$\eta_{solar-to-chem}$
Boujjat et al. (2020b)	Spouted bed	1.5	Directly	Continuous	Steam	Beech wood particles	0.87	1.13	19.4–21.8%	
Boujjat et al. (2020a)	Spouted bed	1.5	Directly	Continuous	Steam	Solid recovered fuels	0.88	1.04	15.8%	
					Steam + O_2[a]		0.79	0.78	11.9%	
Curcio et al. (2021)	Spouted bed	1.5	Directly	Continuous	Steam + O_2[a]	Beech wood particles	0.84	0.82	23.6%	
			Indirectly				0.86	0.82	15.6%	
Hathaway and Davidson, (2017)	Molten salt	3	Indirectly	Continuous	CO_2	Cellulose	0.47		30% (36%[c])	
Hathaway and Davidson, (2020)	Molten salt	3	Indirectly	Continuous	Steam	Cellulose	0.78	0.9	40% (44%[c])	
Hathaway and Davidson, (2021)	Molten salt	3	Indirectly	Continuous	Steam	Cellulose particles	0.93	0.98	45%	
					Steam + O_2[a]		0.99	0.77	41%	

[a]hybrid solar-autothermal operation.
[b]sensible heat included.
[c]based on reacted feedstock.

feedstock's initial molar carbon content that has been transformed to carbon-containing gases such as CO, CO_2, and CH_4:

$$X_C = \frac{n_{CO} + n_{CO_2} + n_{CH_4}}{n_{C,\,feedstock}} \tag{18}$$

For CO_2 gasification, the numerator needs to be subtracted by gas agent CO_2 input. The calculation difference between Eq. 17 and 18 is due to soot production. The energy upgrade factor, U, is defined as the ratio of the heating value of the syngas produced to that of the feedstock:

$$U = \frac{m_{syngas} \cdot LHV_{syngas}}{m_{feedstock} \cdot LHV_{feedstock}} \tag{19}$$

The equilibrium composition for the stoichiometric system $C + H_2O$ at 1300 K is an equimolar combination of H_2 and CO, yielding $U = 1.33$ for solar steam gasification (Gregg et al., 1980a). When the energy content of the products exceeds that of the feedstock, the energy upgrade factor U is more than one, indicating that solar energy has been effectively stored in the products. Obviously, for autothermal gasification, $U < 1$. The solar reactor's solar-to-fuel energy conversion efficiency, $\eta_{solar-to-fuel}$, is defined as the proportion of the energy input that is transformed into the chemical energy of the produced syngas (Piatkowski et al., 2011; Abanades et al., 2021). It represents the global efficiency as both solar irradiative power and calorific content of feedstocks are considered as the input.

$$\eta_{solar-to-fuel} = \frac{m_{syngas} \cdot LHV_{syngas}}{Q_{solar} + m_{feedstock} \cdot LHV_{feedstock}} \tag{20}$$

It is worth noting that many authors (Piatkowski et al., 2009; Wieckert et al., 2013; Kruesi et al., 2014; Müller et al., 2017; Muroyama et al., 2018; Dai et al., 2022) considered $m_{feedstock}$ as reacted biomass feedstock. It is implied that the unconverted solid particles are captured and returned to the reactor for further conversion or other beneficial use. The definition of $\eta_{solar-to-fuel}$ excludes the sensible heat of the hot product gases departing the reactor, which may be recovered and utilized to generate steam, for example. The optical efficiency of the solar concentrating system, which is approximately 70% for a solar tower configuration, is not included in the description as well (Wieckert et al., 2013). In some literatures, another form of efficiency formula is defined as the fraction of solar energy chemically stored in product gas (Gregg et al., 1980b; Kodama et al., 2002):

$$\eta_{solar-to-chemical} = \frac{\Delta H_{reaction}}{Q_{solar}} \tag{21}$$

To be specific, for steam gasification:

$$\eta_{solar-to-chemical} = \frac{n_{CO} \cdot \Delta H_1 + n_{CO_2} \cdot \Delta H_2}{Q_{solar}} \tag{22}$$

where ΔH_1 and ΔH_2 are the standard enthalpy of reaction (11) and (12), respectively. For CO_2 gasification:

$$\eta_{solar-to-chemical} = \frac{0.5 n_{CO} \cdot \Delta H_3}{Q_{solar}} \tag{23}$$

Detailed information on performance indicators for solar thermochemical fuel processes was provided by (Bulfin et al., 2021).

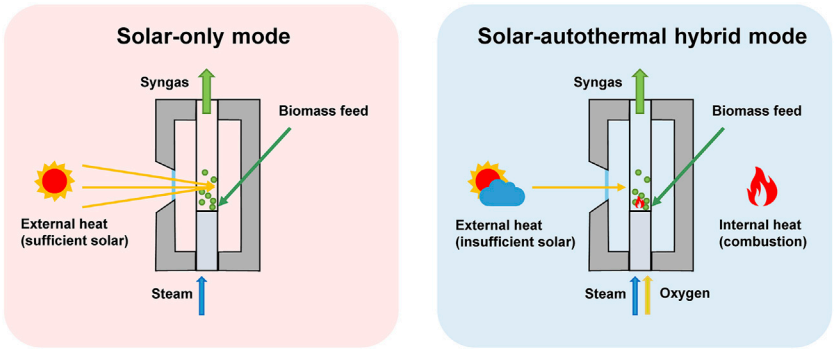

FIGURE 12
Schematic of solar/autothermal hybrid gasification (SAHG) in a cavity reactor.

3.3 Solar gasifier design

Solar gasifier design is the most prominent technology in solar biomass gasification to maximum energy efficiencies. Because the largest cost component arises from the investment of the solar collecting and concentrating infrastructure, a greater $\eta_{\text{solar-to-fuel}}$ implies a smaller solar concentrating system for the same syngas production, which immediately correlates to lower particular syngas fuel cost. The majority of solar gasification research has been carried out at the lab and pilot scales, with seldom commercial applications. Cavity receiver-reactors are often adopted in high-temperature solar-driven biomass gasification reactions.

Depending on the method of heating the reactants, solar cavity reactors can be divided into two categories: 1) directly irradiative reactors, where high-flux solar radiation is directly focused at the biomass feedstocks, and 2) indirectly irradiative reactors, where the radiation strikes an intermediate medium such as an opaque wall, which in turn heats biomass particles in the reaction zone by heat transfer. Directly irradiated solar gasifiers witness higher mass and heat transfer rates, and enable reaching and maintaining high operating temperatures (1,000–1,500°C), which is beneficial to gasification kinetics. However, to allow the focused sunlight to reach the reaction zone, a transparent window is required. The window configuration suffers from potential contamination by tar, biomass particles and condensed gases and its mechanical resistance is another concerning problem under high temperature and pressure conditions, especially at large scales. Conversely, indirect irradiative reactors can solve the aforementioned difficulties while sacrificing heat transfer performance. It sets certain strict limits on the absorber's materials in terms of operating temperature, chemical stability, thermal conductivity, radiative absorptance, and thermal shock resistance (Kruesi et al., 2014). Due to its beneficial characteristics, such as its high emissivity, high thermal conductivity, inertness at high temperatures, and low coefficient of thermal expansion, SiC is frequently employed as an absorbing material (Muroyama et al., 2018). Based on the type of gas-solid contact, the solar gasifiers may be also classified into packed-bed, fluidized-bed, entrained flow, vortex flow, spouted bed, two-zone and molten salt-based gasifiers. As illustrated in Figure 4, a variety of combinations of directly/indirectly irradiative and gas-solid contact reactors has been proposed and tested.

3.3.1 Packed-bed gasifier

Packed-bed gasifiers were the first to be applied in solar biomass gasification (Gregg et al., 1980b; Taylor et al., 1983; Flechsenhar and Sasse, 1995). They are primarily made up of a cavity-type receiver filled with carbonaceous materials. The concentrated solar energy is received directly through a transparent window (Gregg et al., 1980b; Taylor et al., 1983; Flechsenhar and Sasse, 1995; Arribas et al., 2017) or indirectly through an emissive plate re-emitting the radiation (Piatkowski et al., 2009; Müller et al., 2018). Figure 5 shows a schematic of the indirectly irradiated solar packed-bed reactor. Because of the extended residence period and the presence of a substantial amount of carbonaceous material in the reactor that absorbs radiation, these reactors provide a high reaction extent. They are capable of processing feedstocks with large particle sizes and diverse compositions. The thickness of the bed, on the other hand, is a limiting factor for the scaling up of those reactors since its thermal inertia can lead to significant temperature gradients and nonhomogeneous reactions due to limitations in heat and mass transfer, which have a serious influence on the reaction rate (Piatkowski and Steinfeld, 2008).

One of the most typical indirectly irradiative packed-bed reactors was demonstrated by (Piatkowski and Steinfeld, 2008): The solar reactor consists of two cavities, the top one functioning as a radiative absorber and the bottom one housing the reacting packed bed that shrinks as the reaction proceeds, split by a SiC-coated graphite plate. Solar steam gasification of several types of

carbonaceous feedstocks was tested in a 5-kW solar reactor prototype, in which the peak solar-to-fuel efficiencies ranged from 15.9% to 29% based on reacted feedstocks (Piatkowski et al., 2009). The most current study findings on the co-production of syngas and potassium-based fertilizer from agricultural wastes through solar gasification with the same reactor prototype were given by (Müller et al., 2018). A maximum solar-to-fuel efficiency of 17.9% was achieved with 23% potassium content stored in the ash, offering an effective and sustainable process for converting agricultural wastes into useful fuels and nutrients for soil.

As for directly irradiated packed-bed gasifier, recently, (Arribas et al., 2017), conducted solar pyrolysis and solar gasification of low-grade carbonaceous feedstocks (Scenedesmus algae, wheat straw and sewage sludge) under the direct irradiation of a high flux solar simulator. The result showed gasification provided higher production of CO and H_2 and smaller amount of CO_2 and CH_4 than pyrolysis for each kind of feedstock. However, the performance metrics of this reactor were not given.

3.3.2 Fluidized-bed gasifier

In a fluidized-bed gasifier, the dispersed biomass particles provide a larger surface area for thermochemical reactions. Fluidized-bed gasifiers can be further classified into the bubbling ones and circulating ones. Bubbling fluidized-bed reactors have a lower gas velocity than circulating ones with pneumatic flow enhancement (Fang et al., 2021). Compared to packed-bed gasifiers, superior heat and mass transfer is an advantage of fluidized-bed gasifiers. This reduces the level of hot spots generated by non-uniform concentrated solar fluxes (Li et al., 2020b). The fluidized-bed gasifiers have been extensively researched since last century (Taylor et al., 1983; Murray and Fletcher, 1994).

(Müller et al., 2003) experimentally investigated the reaction kinetics of solar steam gasification of coal in a directly irradiated fluidized-bed tubular gasifier. At temperatures over 1400 K, syngas comprising an equimolar combination of H_2 and CO and less than 5% CO_2 was generated. With an energy upgrade factor of 1.34, the solar steam gasification provided a feasible method for solar fuel production. Later on, (von Zedtwitz and Steinfeld, 2005; von Zedtwitz et al., 2007), developed a numerical model to simulate the above-mentioned process. The model employs the Monte Carlo ray-tracing approach to solve the 3-D radiative exchange problem, as well as Langmuir–Hinshelwood rate laws for reaction kinetics.

(Kodama et al., 2002) studied the bubbling fluidized-bed gasification of Australian bituminous coal with CO_2. The fluidized coal bed was directly irradiated using a concentrated Xe-arc lamp beam. The maximum solar-to-chemical energy conversion of 8% was achieved at the optimal gas velocity for fluidization. Because of the tiny reactor employed, it was unable to achieve greater energy conversion efficiencies due to the significant heat losses caused by heat conduction and convection. In a subsequent work, a directly irradiated bubbling fluidized-bed reactor was built and tested for the CO_2 gasification of coal coke (Kodama et al., 2010). It adopted the idea of beam-down configuration, and a high flux solar simulator was utilized to simulate concentrated solar irradiation. Direct contact between the reacting particles and the transparent window was minimized by the relatively large distance between the fluidized bed and the window. Peak solar-to-chemical conversion of 14% was observed under experimentally determined optimum conditions. With increasing gas velocity, the heat transfer in the fluidized bed is enhanced but at the same time the heat loss by sensible heat carried in the exist gas is increased. According to the temperature distribution analysis, the author concluded that the high-temperature reaction zone was likely to be limited to the bed surface.

(Gokon et al., 2012) improved the aforementioned reactor by adding a draft tube at the center of the fluidized particle bed inside the reactor. As depicted in Figure 6, gases can enter the draft tube and the annular area between the inner tube and the reactor shell through separate inlets. In this internally circulating fluidized bed reactor, the feedstock particles constantly migrate downwards in the annulus area and upwards in the inner draft tube. Thanks to this forced circulation pattern, concentrated solar energy could be transferred from the bed surface to the bottom. During CO_2 gasification, a peak solar-to-chemical conversion efficiency of 12% was obtained and a carbon conversion of 73% was reached with a power input level about 3 kW_{th}. Steam gasification was also carried out under the same reactor setup, with a peak solar-to-chemical conversion of 9.7% (Gokon et al., 2015). Afterwards, chemically inert and inexpensive quartz sand was added as a heat transfer and storage medium to keep the bed height constant throughout gasification (Gokon et al., 2014). Some years later, continuous feeding and gasification of coke particles was realized (Gokon et al., 2019). The reactor with a simplified distributor layout achieved a solar-to-chemical conversion of 11.0–13.2% and a carbon conversion of close to 80%.

Regarding indirectly irradiated fluidized bed gasifiers, most recently, (Li et al., 2021b), developed a clapboard-type internally circulating fluidized bed (ICFB) solar reactor. The reactor is made up of a clapboard-type ICFB and an absorption cavity, where a SiC emissive plate absorbed incident concentrated solar energy. Heat transfer between the bed particles and the wall surface can be considerably improved as a result of internal particle circulation, so the risk of overheating is effectively mitigated. CO_2 gasification of charcoal was also experimentally conducted under Singapore's first 28-kW_e HFSS (Li et al., 2020a), where an average carbon conversion of 0.53, an energy upgrade factor of 0.88, and a solar-to-fuel conversion efficiency of 5.3% (sensible heat included) were obtained. It was pointed out that the restricted biomass

feeding mass and the particle entrainment had limited the performance.

3.3.3 Entrained flow gasifier

Entrained-flow (drop-tube) gasifiers are well-suited for usage in indirectly irradiative reactors. Typically, a cavity receiver with or without a window at the aperture plane houses a set of tubular absorbers in an entrained-flow gasifier. Figure 7 shows, schematically, the geometrical configuration. In the tubes, the carbonaceous particles react with gas agent in gasification process.

Two prototypes of this kind of reactors were developed: 1) a 5 cm diameter cylindrical cavity-type receiver containing a 2.5 cm diameter SiC tube (Melchior et al., 2009); 2) an 18 cm diameter cylindrical cavity-type receiver containing five 2.54 cm diameter tubular absorbers (Lichty et al., 2010). For the single-tube solar reactor (Melchior et al., 2009), due to the low feeding rate of charcoal and the comparatively low carbon conversions, the gasification process utilized less than 1% of the solar input. As no efforts were made to optimize the structure of the prototype reactor, the peak observed solar-to-chemical energy conversion efficiency was just 1.53%. For the multiple-tube solar reactor (Lichty et al., 2010), the on-sun trials revealed an average biomass conversion of 58.4%.

3.3.4 Vortex flow gasifier

Another proposal is a directly irradiated horizontal cylinder in which the feedstock and gas are fed in such a way that a vortex flow forms inside the reactor, prolonging the particle residence time. Z'Graggen et al. designed a directly-irradiative 5-kW prototype vortex flow gasifier, where the steam gasification of petcoke was experimentally studied. *Via* the use of an aerodynamic protection curtain made of a tangential flow through four tangential nozzles paired with a radial flow through a circular gap, the window is actively cooled and maintained free of particles or condensable gases. The energy conversion efficiency $\eta_{\text{solar-to-chemical}}$ was between 4.8% and 8.6% for separate feeding of dry petcoke particles and steam, and between 0.5% and 4.7% for petcoke–water slurry feeding (Z'Graggen et al., 2006; Z'Graggen et al., 2007). Heat losses are mainly caused by attenuation, re-radiation, and conduction through the reactor walls.

By swapping out the window for a SiC cavity, Müller et al. transformed the directly-irradiated configuration into an indirectly-irradiated one, as shown in Figure 8 (Müller et al., 2017). In a high-flux solar simulator, gasification of charcoal-water slurry was performed at a concentration ratio of 3,718 suns. A maximum solar-to-fuel energy conversion of 19.7% and nearly complete conversion (X_C = 0.97) in less than 5 s were achieved. The calorific value of the feedstock was increased by 16–35% throughout all 51 solar runs.

Heat and mass transfer are improved in vortex flow and entrained flow reactors, but the residence time is dramatically reduced, placing severe limitations on feedstock size.

3.3.5 Two-zone gasifier

In order to overcome the residence time and particle size restrictions of entrained flow gasifiers while maintaining the benefit of efficient radiative heat transfer, a two-zone reactor concept was first proposed by (Kruesi et al., 2013). It consists of a quick, high-temperature pyrolysis zone that produces limited quantities of tars and highly reactive char and a slow reaction zone that provides enough residence time for char gasification. The gasifier was constructed with a drop-tube zone for rapid pyrolysis and a trickle bed for char gasification. The trickle bed employed structured packing to manage the overall porosity of the gasification zone, making the char particles stay longer while yet allowing radiation to pass through. The performance of the two-zone reactor was experimentally evaluated and compared to the traditional drop-tube arrangements (Kruesi et al., 2014). Using Brazilian sugarcane bagasse particles as feedstock, the result showed a peak carbon conversion rate of 90%, energy upgrade factor of 1.06 and solar-to-fuel conversion efficiency of 21.6% (based on reacted feedstock).

(Bellouard et al., 2017b) experimentally evaluated the performance of a 1 kW two-zone (combined drop-tube and packed-bed) gasifier (Figure 9). A SiC reticulated porous foam is put within the tube at the bottom of the heated zone to trap the biomass in the area where the gasification reaction occurs, ensuring complete conversion while allowing the produced gas to go through. During continuous solar gasification of wood biomass, a high carbon conversion rate of up to 93.5% was achieved. Maximum solar-to-fuel energy conversion efficiency of 28% was attained with wood biomass at 1,400°C, and cold gas efficiency (energy upgrade factor) up to 1.21 was also achieved.

Very recently, an improved updraft solar reactor was developed, constructed, and experimentally tested by (Dai et al., 2022). Based on previous two-zone reactor designs, they improved the structure and operation pattern by changing the moving directions of the reactants. The feedstock was fed from the top of the reactor, and the gas agent was injected from the bottom. In this context, the high-temperature produced syngas can be used to preheat feedstock particles, as the feedstock and gases travelled counter currently in the tube, raising the temperature and reaction rate of pyrolysis. Utilizing lignite coal as feedstock, carbon conversion rates (X_C) were 50–70%. Energy upgrade factor (U) of 1.14–1.17 and solar-to-fuel conversion efficiency of 20%–24% were also achieved based on reacted feedstock.

3.3.6 Spouted bed gasifier

In a spouted bed gasifier, a gas jet entrains solid particles from the bottom from the central area to the bed's peripheral surface; the particles then reach the annular zone due to gravity (Abanades et al., 2021). A 1.5 kW solar conical spouted bed reactor (Figure 10) was designed and experimentally investigated at CNRS-PROMES (Bellouard et al., 2017a). An optional emitter plate was applied to switch the heating mode (directly or

indirectly irradiated). Wood particles were continuously delivered into the reactor and successfully gasified at 1,100–1,400°C under real concentrated radiation. Parametric studies of the gasification conditions were carried out to optimize the syngas production. The influence of temperature, oxidizing agent, reactants stoichiometry, heating mode, biomass type, particles size, and biomass feeding rate on gasification performance was studied (Chuayboon et al., 2018a; b; Boujjat et al., 2019b; Chuayboon et al., 2019). Carbon conversion rates over 94% and an energy upgrade factor of up to 1.21 were achieved (Bellouard et al., 2019). To increase the thermal inertia of such type solar reactors, a layer of inert particles (alumina, SiC, olivine, and sand) has also been introduced and studied (Boujjat et al., 2020b).

3.3.7 Molten salt gasifier

It was reported that molten carbonate salts could function as a combined catalyst and heat transfer medium for solar CO_2 (Matsunami et al., 2000) or steam gasification (Hathaway et al., 2011). (Hathaway et al., 2013a) undertook a study to determine the ability of molten carbonate salts to improve the overall conversion of diverse cellulosic feedstocks into syngas through gasification processes. The feedstocks were gasified using steam in inert gases and in molten salts, respectively. At 1200 K, the addition of molten salts boosted overall syngas output by 25.7% and the reactivity index by up to 490%. Secondary products, such as condensable tar, were cut by 77%.

In a subsequent work, a 2.2 kW prototype molten salt gasifier (Figure 11) was studied under simulated concentrated solar radiation (Hathaway and Davidson, 2017). The inner cylinder is a cavity receiver with a front aperture. The outer cylinder bounds an annular volume which contains the molten salt and reacting biomass. Utilizing cellulose as biomass feedstock and CO_2 as gas agent, the reactor obtained a solar-to-fuel efficiency of 30% and converted 47% of the carbon in a continuous process at 1218 K. The pneumatic feed system's requirement for an extra gas stream led to the entrainment of char, which was the cause of the poor carbon conversion rate. Afterwards, a novel extrusion/screw conveyor feed system was applied (Hathaway and Davidson, 2020). Steam gasification of cellulose was carried out based on this new feed system, with the carbon conversion rate reaching 78%. At 1208 K, a solar-to-fuel efficiency of 40% was achieved, which was the highest value reported for a solar gasifer in the literatures.

3.3.8 A brief summary on solar gasifier designs

In short, different solar reactor designs were experimentally tested for solar biomass gasification including packed-bed, bubbling fluidized-bed and entrained flow reactors. More recently, internally circulating fluidized-bed, vortex-flow, spouted-bed, two-zone and molten salt-based gasifiers have been considered. Table 2 compares the performance of the most important reactor designs for solar gasification of carbonaceous feedstock. Because there are differences in how the energy conversion efficiency is recorded, special attention should be paid when making direct comparisons.

Generally speaking, the packed-bed reactor design is distinguished by its durability, simplicity of operation, and ability to handle feedstock particles with different sizes and diverse compositions without any prior treatment, while it faces challenges with heat and mass transfer. Additionally, all previous packed-bed experiments were conducted in a batch-mode. Fluidized beds are widely accepted in combustion and gasification applications, as they enable continuous operation (Huang et al., 2012; Xue et al., 2015; Muroyama et al., 2018), quick adjustment of inputs, long particle residence periods, and sufficient gas-solid contact with effective heat and mass transfer. One disadvantage of fluidized-bed designs in comparison with packed beds is the requirement for smaller, generally homogenous feedstock particles, which results in more expensive feedstock preparation. Particle entrainment may have limited carbon conversions. Heat and mass transport are improved in vortex flow and entrained flow reactors, although residence time is dramatically reduced, imposing strict requirements on the feedstock size. The two-zone (combined drop-tube and packed-bed) design increases the effective residence time of char particles while still providing the efficient heat transfer to the particles needed for fast pyrolysis. Conical spouted bed reactors are more adaptable and capable of handling uniform or irregular particle distributions, coarse particles, and particles of various types than fluidized-bed reactors. Molten salt provides performance advantages over operation in gaseous environments. It acts as a heat transfer medium, catalyzes gasification reaction, promotes tar cracking, and the thermal mass allows for steady syngas production during solar transients. Nevertheless, molten salt related creep or corrosion issues need to be carefully considered. Separation procedure is also required for the solid residue (char/ash) and molten salt mixtures.

4 Solar intermittence management

When it comes to the rising interest in continuous syngas production, solar gasification technology is hampered by the inherent problem of intermittent solar radiation caused by cloud and rain. It was argued that the problem could be alleviated with thermal storage or hybridization (Hathaway et al., 2013b). Specifically, three main approaches have been investigated to manage solar intermittence: 1) performing solar/autothermal hybrid gasification in cavity gasifiers, 2) integrating dual fluidized-bed gasifier with solar particle receivers, and 3) Adopting intermediate heat transfer fluids. Solar intermittence management is a crucial step towards the usage of the technology during overcast times or overnight in a commercial plant for production of renewable solar fuels.

4.1 Solar-autothermal hybrid gasification in cavity gasifiers

4.1.1 Concept and simulation

Based on aforementioned cavity solar reactors, the concept of solar/autothermal hybrid gasification (SAHG) has been proposed to combine conventional autothermal gasification and solar-driven operation together to satisfy the need for continuous syngas production. The hybrid solar/autothermal reactor operates in three general modes: 1) sole solar-driven gasification during periods of sufficient DNI, 2) autothermal gasification only for night operation, and 3) an integrated system for periods of insufficient DNI. In the autothermal gasification mode, a part of the feedstock ϕ (also called equivalence ratio) is combusted (Eq. 24) to drive the endothermic gasification (Eq. 25).

$$\phi \cdot | \ CH_xO_y + \left(1 + \frac{x}{4} - \frac{y}{2}\right)O_2 \rightarrow \frac{x}{2}H_2O + CO_2 \tag{24}$$

$$(1-\phi) \cdot | \ CH_xO_y + (1-y)H_2O \rightarrow \left(1 + \frac{x}{2} - y\right)H_2 + CO \tag{25}$$

In cavity-type reactors, O_2 can be easily injected with gasification agent through the gas inlet, which simplifies the intricate interaction and control of the various system components. Figure 12 shows a schematic diagram of SAHG in a cavity reactor.

(Muroyama et al., 2014) developed a simplified dynamic model to analyze fluidized steam solar/autothermal hybrid gasification considering DNI variations due to the changing weather, combining heat transfer with chemical equilibrium predictions. To maintain a specified temperature, the flow of O_2, H_2O, and carbonaceous material delivered into the system was dynamically controlled to solve DNI inadequacies. For a 5-day simulation with transient solar fluctuations, the temperature control error was no more than 4.3°C. Using lignite coal as the feedstock, an energy upgrade factor of 1.2 and a solar-to-fuel efficiency of 39% were achieved in solar-only mode, while the cold gas efficiency maintained at 87% in autothermal mode.

(van Eyk et al., 2016) developed a 1-D mathematical model to investigate the solar/autothermal hybrid gasification of coal particles in an entrained-flow reactor, including autothermal, solar-only, and combined cases. The overall solar-to-fuel efficiency rose from autothermal case to solar case, however for majority of solar input values (less than 3 MW/m^2), the reactor efficiency was even lower than autothermal gasification due to the additional re-radiation heat loss. It is worthwhile to note that the increase in the energy upgrade factor for these low solar input cases can still be beneficial.

An ICE CCHP system powered by SAHG was thermodynamically investigated by (Li et al., 2018). Based on Gibbs free energy minimization, a zero-dimensional steady-state model of the SAHG in an indirectly irradiated two-cavity reactor was developed. Under different solar inputs, the optimal steam-to-feedstock and oxygen-to-feedstock ratios were first calculated and then applied to control feeding mole flow rates of the gas reactants during hybrid operation.

A dynamic numerical model of a scaled-up solar gasification reactor was established by (Boujjat et al., 2020c), where both solar-only and hybrid solar/autothermal modes were examined. Three feeding strategies were proposed and compared. The first is a straightforward on/off control method. The second approach is to adjust the biomass and steam flow rates to maintain the reactor temperature at 1,200°C. The third one employs pure oxygen and extra biomass injection to compensate for solar disturbances, ensuring constant day and night syngas production. It was shown that the third mode resulted in the most stable process operation under varying solar power input, while ensuring continuous conversion of biomass at night and during overcast times.

4.1.2 Lab-scale experimental test

Lab-scale experimental tests for SAHG have been carried out using fluidized-bed, spouted bed and molten salt reactors. (Muroyama et al., 2018) first tested SAHG in a prototype 1.5 kW_{th} indirectly irradiated fluidized-bed gasifier. The experiment revealed the ability to increase temperatures by injecting pure oxygen into the solar gasifier. Transient solar energy deficiencies inherent in solar gasification could thus be solved. The negative effects of combustion were also observed to be significant, with O_2:C lowering the H_2:CO ratio, cold gas efficiency, solar-to-fuel efficiency, and increasing CO_2 output. As a result, the injection of pure oxygen should be minimized in SAHG unless necessary. In solar-autothermal hybrid operation mode, highest solar-to-fuel efficiency of 15.4% was observed using activated charcoal as feedstock, and the corresponding carbon conversion rate and energy upgrade ratio were 0.79 and 0.74, respectively.

Recently, (Hathaway and Davidson, 2021), conducted hybrid operation in their modified molten salt gasifier. They found that steam addition could control the produced syngas quality (*via* water-gas shift reaction). In solar-only mode, solar gasification operated with a stoichiometric amount of steam at 1225 K and concentration ratio of 1,350 suns, showing a solar-to-fuel efficiency of 45% and a feedstock conversion rate of 93%. Hybrid operation with the addition of O_2 was performed when the solar input was reduced by 23% while maintaining the feedstock flow rate, achieving 41% energy efficiency and 99% carbon conversion. The *in-situ* WGS ensured a hydrogen and carbon monoxide ratio of 1.7:1 in the product gas stream, at the expense of nine times the stoichiometric amount of steam consumption.

Spouted bed gasifiers were also tested in solar-only and mixed solar-combustion mode under real concentrated solar flux and the effects of process hybridization on syngas yield and reactor performance were investigated (Boujjat et al., 2019a).

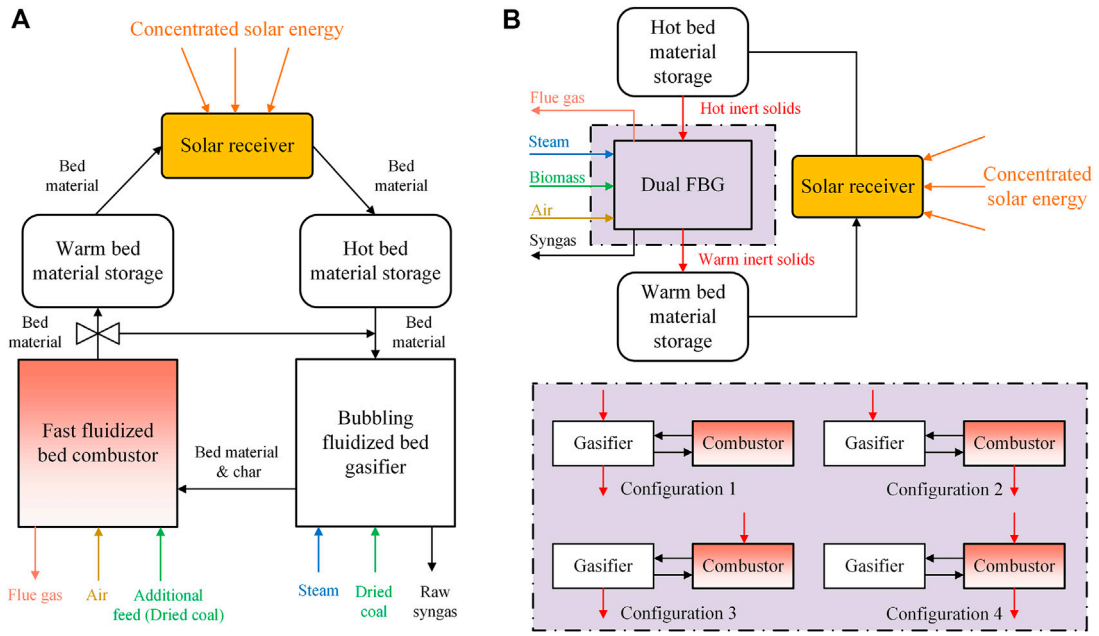

FIGURE 13
Layout of SDFB system with thermal storage **(A)** adapted from (Guo et al., 2015) **(B)** adapted from (Gómez-Barea et al., 2021).

The results confirmed that O_2 feeding rate is a relevant variable to control the process temperature. Most recently, (Curcio et al., 2021), parametrically studied the impact of oxygen flow rate, combination of oxidizing agents, reaction temperature and heating mode (directly/indirectly irradiated) on SAHG performance in a conical spouted bed gasifier. They also provided useful information on thermal and chemical transient behaviors during the switch in operating mode between solar-driven and hybrid gasification.

4.2 Integration of dual fluidized-bed gasifier and solar receiver

Dual fluidized-bed (DFB) gasifiers have been well developed for autothermal biomass gasification (Karl and Proell, 2018; Hanchate et al., 2021). A DFB system consists of a gasifier (typically bubbling fluidized-bed) where the biomass is injected, devolatilized and the char is partially gasified with steam, and a combustor (typically fast fluidized-bed) where the char coming from the gasifier is burned with air. To be clear, the heat generated from combustion is transferred to the gasifier by sensible heat of the circulating solids.

(Guo et al., 2015) proposed the concept of solar hybridized DFB (SDFB), by integrating DFB with a solar particle receiver. In such system, the heat needed for the gasification process is transferred from the combustion site and/or the solar receiver using the solid bed material as a heat carrier. Due to their possible low cost and high working temperatures (>1,000°C), solid particles are thought to be ideally suited for use as solar thermal heat carriers and storage media. As depicted in Figure 13A, the bed materials performed a complete loop between the warm storage tank, the solar receiver, the hot storage tank, the gasifier and the combustor. The flow direction and flow rate of the bed materials were controlled to accommodate the variation in solar radiation. In a subsequent study, a novel configuration of solar hybridized DFB gasification process was presented with char separation for the production of Fischer-Tropsch (FT) liquids (Guo et al., 2017). Three approaches to further improve the energetic and environmental performance of the system were proposed and assessed: 1) char separation from the bubbling fluidized gasifier; 2) co-gasification of biomass and lignite; 3) FT reactor tail-gas recycle.

Based on the SDFB concept, (Gómez-Barea et al., 2021), simulated SDFB biomass gasification performance with a pseudo-equilibrium model, considering 4 different configurations for introducing/extracting the solids in the system (Figure 13B). For a standard configuration (Configuration 1), the process can be performed efficiently in a SDFB gasifier with char conversion of up to 80%, corresponding to an average 28-min char resident time. The operation required 2.4 MJ/kg_{bio} of solar energy input, producing syngas with 12% of solar share (defined as the ratio between the solar heat supplied to the system and the lower heating value of the syngas).

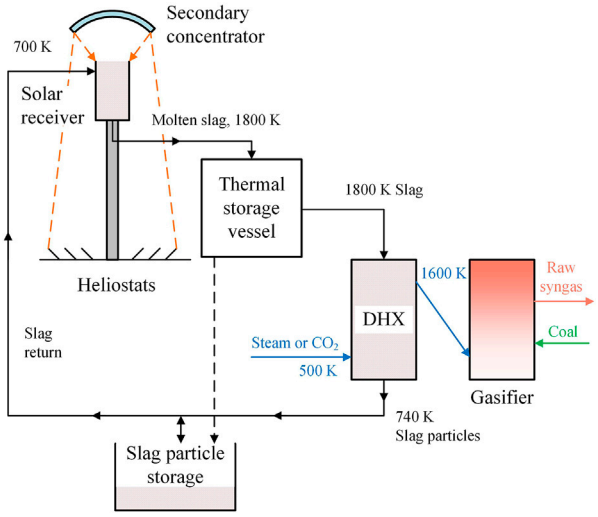

FIGURE 14
Adoption of molten slag as heat transfer medium. Adapted from (Bruckner, 1985).

In another work, the annual performance of the same system with char separation and storage was numerically investigated (Suárez-Almeida et al., 2021). To increase the solar share for a given char conversion at constant gasification temperature, the char from the solids stream leaving the gasifier can be separated and stored, thus decreasing the char burned in the combustor; under this operational mode, the solar heat has to compensate the heat from char combustion. The simulation result showed the seasonal char storage would be a potential option for increasing the flexibility of the system.

To conclude, the advantage of SDFB concept is that the solar receiver and the reactor are not coupled, while heat transfer is particularly efficient since carrier particles are employed directly in the reactor. Large-scale solid fuel gasification and liquid fuel generation may be solved by such combination (Tregambi et al., 2021). However, in such system, the removal of solid particles from the gasifier will theoretically lead to reactive particles in the solar loop, which may well present additional issues. Besides, the gasification unit in SDFB needs to be modified and improved in solar mode, since the residence time is too long (>20 min) compared with that of current conventional DFB gasification (1–5 min). Up to now, only theoretical and numerical studies have been carried out on this integration, and experimental studies are needed to further prove this concept.

4.3 Adoption of intermediate heat transfer media

Adopting an intermediate transfer medium increases operational flexibility and makes it possible to use a larger variety of contacting configurations. The associated surface areas can now be distributed across a bed's volume rather than being mostly determined by the particle surface. A temporary storage also smooths out the erratic solar energy supply (Nzihou et al., 2012).

In 1985, (Bruckner, 1985), designed a solar coal gasification plant using molten slag as the heat transfer and storage medium. As illustrated in Figure 14, a glassy, synthetic slag was delivered to the top of the solar receiver, being heated to 1800 K by the concentrated solar energy. The melted liquid slag flowed into a thermal storage vessel before being gravity fed to the direct contact droplet heat exchanger (DHX). In DHX, feed gas (CO_2 or steam) was heated to very high temperatures to drive coal gasification in a follow-up gasifier. With a nominal daily irradiation of 8 h assumed, the receiver duty cycle is 33%. As a result, the solar receiver has been designed to be three times the thermal input needed by the gasifier, allowing for simultaneous charging of a 16-h storage vessel.

Similar to Bruckner's concept, a continuous hydrogen generation system was suggested and demonstrated by (Xiao et al., 2013). It utilized molten salts-stored solar energy to drive biomass gasification in supercritical water. In the experimental study, salts were first heated with an electrical heater simulating a solar receiver system. Then, salts flowed to a helical concentric tube heat exchanger, where the slurry of biomass flows through the inner tube and the molten salts through the external tube in a countercurrent flow. When salts finished the cycle, they returned to the molten salt storage tank, and then they can be heated again in the electrical heater. In this reactor, hydrogen-rich gas was effectively produced by gasifying both model compounds and actual biomass (corn cob).

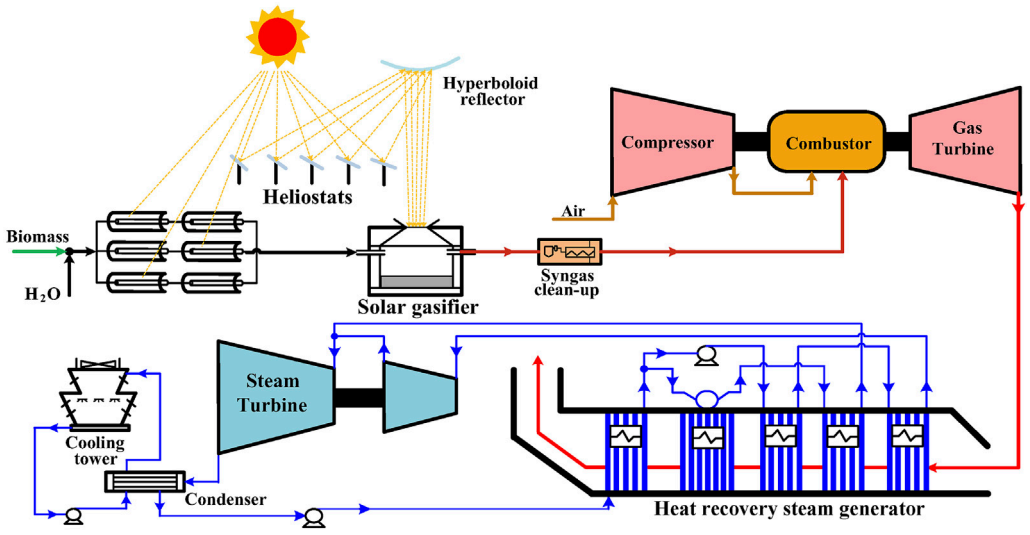

FIGURE 15
Solar biomass gasification in a combined cycle power generation system. Adapted from (Bai et al., 2017).

5 Subsequent utilization of synthesis gas (downstream applications)

Syngas produced by solar assisted biomass gasification can be used as solar fuels in power cycles (Liu et al., 2021). It is also favorable to be utilized as the raw material to produce synthetic liquid fuels such as methanol, ethanol, dimethyl ether and FT liquids (Jie Ling et al., 2022). Solar thermal energy stored as thermochemical heat can be a convincing approach to promote energy storage at ambient temperatures for long periods of time without heat loss.

5.1 Power generation

(Liu et al., 2016) compared the thermodynamic performance of two solar-biomass hybrid Brayton-Rankine combined cycle power generation systems. The first system employed the thermochemical hybrid routine, named solar gasification combined cycle (SGCC) system, in which concentrated solar energy activated the gasification of the biomass, and the produced syngas was used as a solar fuel in a combined cycle to generate electricity. The second system named solar hybrid combined cycle (SHCC) system adopted the thermal integration concept. The feedstock of biomass was gasified by the typical autothermal gasification technology, while the concentrated solar energy was directly utilized for heating the compressed air within the solar volumetric air receiver. The gasified syngas was combusted with the solar-heated air in the combustor, and the qualified high-temperature gas was used to drive the gas turbine for producing electricity. According to the annual system evaluation, the overall energy efficiency of SGCC system reached to 29.36%, compared with the SHCC system of 28.03%. The SGCC system showed more favorable thermodynamic performance by employing the solar thermochemical routine. (Bai et al., 2017) adopted a two-stage gasification concept in a power generation system, in which mid-temperature solar heat energy was used for biomass pyrolysis, high-temperature solar heat energy for biomass gasification (Figure 15). Simulation results showed the energy level upgrade ratio in the two-stage gasification system for the provided solar thermal energy was 32.35% compared to 21.62% in one-stage setup.

In addition to the combined Brayton-Rankine cycle, the integration of supercritical carbon dioxide power cycle and solar gasification has also been studied by (Xu et al., 2019). This hybridization concept has a potential to achieve both CO_2 capture and a high solar share. According to the simulation, the net energy and exergy efficiency of the proposed system reached 43.4 and 44.6%, respectively.

5.2 Fuel production

5.2.1 Fischer-Tropsch synthesis

The Fischer-Tropsch (FT) process is a well-established and developed method for converting syngas to higher hydrocarbons, particularly liquid transportation fuels. Biomass gasification in conjunction with the FT process is a reassuring and encouraging possibility for producing “green” liquid fuels (Ail and Dasappa, 2016). In the FT synthesis, carbon monoxide is hydrogenated over metallic catalysts producing linear hydrocarbons, according to the following overall reaction:

$$2nH_2 + nCO \rightarrow -(CH_2)_n - + nH_2O \quad \Delta H^0_{250^\circ C} = -158.5 kJ/mol \ (n = 1) \tag{26}$$

Details on reaction mechanism, catalyst selection and reactor design for FT process were reviewed by (Ail and Dasappa, 2016; Konarova et al., 2022). In terms of the study of overall system, Kaniyal et al. developed a quasi-steady state dynamic model to estimate the transient behavior of the hybridized solar gasification of coal and its blend with biomass and natural gas for FT liquid fuel production (Kaniyal et al., 2013a; Kaniyal et al., 2013b). The authors found a 21%–22% annually averaged improvement in the energetic output per unit feedstock compared to that of a non-solar autothermal coal-to-liquid system. Recently, Pye and his colleagues analyzed algae-to-liquid fuel production *via* solar-driven supercritical water gasification (SCWG), reforming and FT processes (Rahbari et al., 2019; Shirazi et al., 2019). The suggested system exhibited a levelized cost of fuel (LCOF) as low as 2.44 USD/L of gasoline equivalent using 2016 as the base year for costing. The price appears to be much higher than that of fossil-based liquid fuels. However, the comparison is not absolutely accurate unless the embodied costs of associated GHG emissions generated by fossil-based fuel production are taken into consideration. In a subsequent work, to achieve the required H_2/CO ratio of two for the FT process, PV-electrolysis based supplemental H_2 was chosen as the preferred alternative, since syngas obtained from biomass can be H_2 deficient (Rahbari et al., 2021). (Zhong et al., 2021) conducted a 3E (energetic, economic, and ecologic) analysis on biomass-to-liquids production system based on solar gasification and FT synthesis. Though not economic-competitive in short term (LCOF is 44.2% higher than market price), the system is still promising when the carbon tax reaches 81.5 USD/t.

5.2.2 Methanol production

Methanol production is another approach to use cleaned syngas to give transport fuel. For this application the H_2/CO ratio must be 2. (Bai et al., 2015) proposed a poly-generation system of generating methanol and power with the solar gasification of biomass. In such system, the syngas from the biomass gasification was used for methanol production in a synthesis reactor, while the unreacted gas was used to generate power *via* a combined cycle power unit. After system scale optimization, the favorable system annual averaged energy efficiency, 48.35%, was achieved with methanol production cost of 361.88 USD/t (Bai et al., 2018, 2019).

Recently, (Xin et al., 2022), integrated solar-driven coal gasification with a methanol and electric power poly-generation system using a direct-fired supercritical carbon dioxide power cycle (Allam cycle) for power generation and carbon capture. The solar integration could improve the methanol production and net power output by 94.2% and 22.9%, respectively. The levelized cost of methanol was obtained as 341.95 USD/t.

5.2.3 Hydrogen production

Experimental tests for solar gasification of biomass in supercritical water (SCW) was successfully carried out by researchers in Xi'an Jiaotong University. The maximum reaction temperature of the solar reactor enclosed by a quartz glass window reached 650°C, which was sufficiently high enough to realize biomass gasify completely in SCW (Liao et al., 2013). Hydrogen fraction in the gas product also reached to 50% (Chen et al., 2010). The encouraging results indicated that hydrogen production with SCWG of biomass using concentrated solar energy was a promising approach.

(Lu et al., 2011) conducted a technical and economic evaluation of solar hydrogen production by supercritical water gasification of biomass. In high pressure separator, CO_2 is separated from product H_2 by high-pressure water absorption because solubility of CO_2 in high-pressure water is much larger than that of H_2. The projected cost of hydrogen production was 38.46 CNY/kg for the experimental demonstration system with the wet biomass treatment capacity of 1 t/h and the total project investment contributed significantly to the hydrogen production cost.

(Wu et al., 2019) proposed a multi-functional system based on solar biomass gasification to produce power, heating and hydrogen. The gasified syngas was used to produce power and heating *via* a power cycle unit during the heating periods and to produce hydrogen *via* a water-gas shift reactor during the non-heating periods. The annual average hydrogen production efficiency of the system reached 64.97%.

5.3 CCHP systems

Solar biomass gasification-based combined cooling heat and power (CCHP) system is another attractive option for downstream applications, as it can realize a cascading utilization of energy with high overall efficiency and low greenhouse gas emissions.

(Li et al., 2018) thermodynamically studied an internal combustion engine (ICE) combined cooling heat and power (CCHP) system driven by the SAHG of biomass. The suggested system was made up of two main subsystems: the SAHG subsystem and the CCHP subsystem. The syngas produced from SAHG powered an ICE to generate electricity along with waste heat of exhaust gas. The exhaust gas released from ICE drove a double-effect absorption chiller (DEAC) to deliver chilled water for cooling. In a subsequent step, hot water was produced using the exhaust gas that had previously passed through the DEAC at a somewhat lower temperature. An annual evaluation revealed that, when compared to the identical CCHP system powered by autothermal gasification, the SAHG system achieved annual average increases in heat, power, and cooling of 19.5%, 23.8%, and 4.5%, respectively.

(Wang et al., 2019) also presented a similar CCHP system while the waste heat from product gas was used to produce steam by heat exchanger to supply biomass gasification. Influences of variable parameters (electricity load ratio and DNI) in the off-

design work conditions were studied. The results of the case study with 100 kW electricity generation indicated that the hybrid CCHP system based on solar biomass gasification achieved average energy and exergy efficiencies of 56% and 28%, respectively, and the increasing ratio of heating value of product gas reached 55.09% compared to autothermal gasification. Recently, (Wu et al., 2020), included an economic analysis in their work to evaluate the technical feasibility of the proposed hybrid CCHP system. When biomass price is assumed to be 40 USD/t, the payback period is 2.70 years in the proposed new system, which is 3.94 years shorter than the reference autothermal system.

6 Challenges and future prospects

6.1 Reactor design and scaling up

As mentioned in Section 3.3, solar reactor design is the most prominent part in solar assisted biomass gasification to maximum energy efficiencies. Despite several solar gasifiers tested at lab-scale, seldom have been scaled-up and none has been commercialized due to high reaction temperature, the large reactor volume needed to accomplish fuel conversion, and the inconsistent syngas production (Tregambi et al., 2021). Up to now, only three types of solar gasifier (packed-bed, entrained flow and vortex flow) have been applied in pilot scale projects.

In cooperation with PSI and ETH Zurich, Holcim (Switzerland) developed a 150 kWth solar gasifier that was based on the idea of an indirectly irradiated packed-bed solar reactor and intended for the batch gasification of biomass and waste feedstocks. The experiment was conducted at the CESA-1 solar tower of CIEMAT's Plataforma Solar de Almeria in Spain (Wieckert et al., 2013). The solar reactor was installed 46 m up atop the solar tower. An array of sun-tracking heliostats guided the sunrays to a chilled mirror above the window, which directed the concentrated solar beam through the cavity. The temperature of the emitter plate rose quickly, whereas the packed bed's poor thermal conductivity slowed the temperature rise towards the bottom of the bed. As a result, heat transport over the porous bed was considered to be the rate-controlling mechanism. Nevertheless, the experiment showed a satisfactory result, with an energy upgrade factor of up to 1.3 achieved, and the solar-to-fuel energy-conversion efficiency varying between 22 and 35%.

Sundrop Fuels Inc. (United States), in collaboration with the University of Colorado, has built a 1-MW solar plant to convert wood waste and other kinds of biomass into syngas. It employed a field of 2,700 mirrors to focus sunlight onto a 20-m solar tower in order to provide the heat required to operate the indirectly irradiated entrained-flow reactor (Service, 2009; Piatkowski et al., 2011). The 300-kW pilot version of the direct-irradiated vortex-flow reactor was also installed by the ETH Zurich, PDVSA (Venezuela), and CIEMAT (Spain) for the gasification of petcoke (Z'Graggen and Steinfeld, 2008; Piatkowski et al., 2011). However, no operating result regarding these two projects can be found in the open scientific literature.

Despite the fact that the concentrated solar assisted biomass gasification system is well-positioned and has several benefits for producing high-quality syngas, it is still in its early stages of development. Several types of solar gasifiers still need optimization and improvement to be scaled up with minimal issues and concerns. Though challenging, scaling up offers prominent advantages, as solar reactor at a large scale has a smaller surface area to volume ratio, which help reduce the heat loss and improve the energy efficiency. A wide variety of large-scale system simulations (Section 5) covering various downstream applications showed that energy and environmental benefits are substantial while the technology remains economically challenging, and requires incentive-based environmental policies.

6.2 Continuous high-quality syngas production

As emphasized in Section 4, solar intermittence management is a crucial step towards the usage of the technology during overcast times or overnight in a commercial plant for production of renewable solar fuels. The proposed SAHG concept has alleviated this problem to a large extent, however, the switch from solar-driven to hybrid (solar/combustion) mode lowers significantly the syngas yield (especially H_2) while increasing CO_2. Furthermore, the observed decline of syngas quality (both heating value and H_2:CO ratio) due to hybridization can be an issue considering downstream applications. The ideal H_2:CO ratio for direct synthesis of DME is unity. The ideal ratio for the synthesis of FT liquids or methanol is two. As the H_2: CO molar ratio drops below one in hybrid mode, control of the product gas ratio is required to pair with fuel or chemical synthesis. Recently, (Hathaway and Davidson, 2021), studied *in-situ* water gas shift in their molten salt reactor, avoiding an additional reactor. It did, however, necessitate a water flow rate nine times greater than the stoichiometric one. Since the WGS reaction is exothermic, from the point of view of the reaction equilibrium, the reaction favors lower temperature. (Curcio et al., 2022) suggested it would be better to maintain a constant total syngas throughput and leave the control of H_2:CO ratio to a downflow shift unit. Instead of water gas shift, (Rahbari et al., 2021), employed PV-electrolysis based supplemental H_2 to adjust H_2:CO ratio. There are few empirical results available in this sector, and the dynamic coupling among the different unit operations is still in its infancy (Boujjat et al., 2020c). Continuous high-quality syngas production together with its downstream processes needs to be further detailed.

In addition, control strategy in SAHG is a crucial factor to the system performance. Different control strategies have been numerically studied to optimize SAHG (Section 4.1.1), but none has been applied in an experimental demonstration, as fixed H_2O:C and O_2:C ratio were usually adopted in concept-proving experiments (Section 4.1.2). In the future, intelligent

algorithms for dynamic control, short-term and accurate forecasts of DNI (Boujjat et al., 2020c), and experimental validations on smart control strategies ought to be investigated.

7 Conclusion

This work presented a comprehensive review of the production of solar fuels from solar assisted biomass gasification. It began by reviewing the background on solar concentrating technologies. The fundamentals and performance metrics of solar biomass gasification were also provided. The state-of-the-art solar gasifier designs were summarized in detail, including classification, characteristics and their corresponding experimental performance. Finally, towards practical applications, strategies for solar intermittence management and downstream utilization of syngas were discussed. Conclusion can be drawn as follows.

- Solar assisted biomass gasification is a promising pathway to produce solar fuels. Compared with autothermal biomass gasification, the usage of high-flux concentrated solar radiation to drive endothermic gasification reactions improves energy efficiencies, saves biomass feedstocks, and is free of combustion by-products.
- Because of their greater concentration ratios, 3-D point-focusing concentrators are more practicable for driving solar gasification. The solar tower system (including beam-down configuration) is becoming more appealing and exhibits a great potential for coupling with large-scale, high-temperature thermochemical processes.
- Cavity receiver-reactors are often adopted in high-temperature solar-driven biomass gasification reactions. A variety of combinations of directly/indirectly irradiative and gas-solid contact reactors has been proposed and tested. Each design has its own characteristics. The ultimate objective is to maximum solar-to-fuel energy conversion efficiency, by optimizing solar heating, minimizing heat losses and adopting proper gas/solid contacting to enhance heat and mass transfer.
- Solar intermittence management is a crucial step towards the usage of the technology during overcast times or overnight in a commercial plant for production of renewable solar fuels. Three directions have been suggested: 1) SAHG operation in a cavity reactor, 2) integration DFB with solar particle receiver, and 3) adoption of intermediate HTFs. The concept of SAHG in cavity reactors has been proved in lab-scale prototypes, while better operation strategy is under development.
- Syngas produced by solar assisted biomass gasification can be used as solar fuels in power cycles. It is also favorable to be synthesized into other transportation fuels such as methanol, FT liquids, and hydrogen. Solar biomass gasification-based CCHP system is another attractive option for its high overall efficiency and low greenhouse gas emissions.
- Nowadays, some intractable issues still challenge applications of the solar biomass gasification technologies, including the design and scaling up of the solar gasifier, the requirement for continuous high-quality syngas production, the collection and transportation of biomass, and the high investment cost of the technology. These problems should be further investigated for accelerating the commercial operation of energy system with solar assisted biomass gasification.

Author contributions

All authors listed have made a substantial, direct, and intellectual contribution to the work and approved it for publication.

Funding

This work is supported by the key project of the National Natural Science Foundation of China under the contract No. 51736006.

Conflict of interest

The authors declare that the research was conducted in the absence of any commercial or financial relationships that could be construed as a potential conflict of interest.

Publisher's note

All claims expressed in this article are solely those of the authors and do not necessarily represent those of their affiliated organizations, or those of the publisher, the editors and the reviewers. Any product that may be evaluated in this article, or claim that may be made by its manufacturer, is not guaranteed or endorsed by the publisher.

References

Abanades, S., Rodat, S., and Boujjat, H. (2021). Solar thermochemical green fuels production: A review of biomass pyro-gasification, solar reactor concepts and modelling methods. *Energies* 14 (5), 1494. doi:10.3390/en14051494

Agrafiotis, C., Roeb, M., and Sattler, C. (2015). A review on solar thermal syngas production via redox pair-based water/carbon dioxide splitting thermochemical cycles. *Renew. Sustain. Energy Rev.* 42, 254–285. doi:10.1016/j.rser.2014.09.039

Agrafiotis, C., von Storch, H., Roeb, M., and Sattler, C. (2014). Solar thermal reforming of methane feedstocks for hydrogen and syngas production—a review. *Renew. Sustain. Energy Rev.* 29, 656–682. doi:10.1016/j.rser.2013.08.050

Ail, S. S., and Dasappa, S. (2016). Biomass to liquid transportation fuel via Fischer Tropsch synthesis – technology review and current scenario. *Renew. Sustain. Energy Rev.* 58, 267–286. doi:10.1016/j.rser.2015.12.143

Arribas, L., Arconada, N., González-Fernández, C., Löhrl, C., González-Aguilar, J., Kaltschmitt, M., et al. (2017). Solar-driven pyrolysis and gasification of low-grade carbonaceous materials. *Int. J. Hydrogen Energy* 42 (19), 13598–13606. doi:10.1016/j.ijhydene.2017.02.026

Bai, Z., Liu, Q., Gong, L., and Lei, J. (2019). Investigation of a solar-biomass gasification system with the production of methanol and electricity: Thermodynamic, economic and off-design operation. *Appl. Energy* 243, 91–101. doi:10.1016/j.apenergy.2019.03.132

Bai, Z., Liu, Q., Gong, L., and Lei, J. (2018). Thermodynamic and economic analysis of a solar-biomass gasification system with the production of methanol and electricity. *Energy Procedia* 152, 1045–1050. doi:10.1016/j.egypro.2018.09.118

Bai, Z., Liu, Q., Lei, J., Hong, H., and Jin, H. (2017). New solar-biomass power generation system integrated a two-stage gasifier. *Appl. Energy* 194, 310–319. doi:10.1016/j.apenergy.2016.06.081

Bai, Z., Liu, Q., Lei, J., Li, H., and Jin, H. (2015). A polygeneration system for the methanol production and the power generation with the solar–biomass thermal gasification. *Energy Convers. Manag.* 102, 190–201. doi:10.1016/j.enconman.2015.02.031

Baruah, J., Nath, B. K., Sharma, R., Kumar, S., Deka, R. C., Baruah, D. C., et al. (2018). Recent trends in the pretreatment of lignocellulosic biomass for value-added products. *Front. Energy Res.* 6, 141 doi:10.3389/fenrg.2018.00141

Basu, P. (2010). *Biomass gasification and pyrolysis: Practical design and theory*. Boston: Academic Press. doi:10.1016/C2009-0-20099-7

Bayon, A., de la Calle, A., Ghose, K. K., Page, A., and McNaughton, R. (2020). Experimental, computational and thermodynamic studies in perovskites metal oxides for thermochemical fuel production: A review. *Int. J. Hydrogen Energy* 45 (23), 12653–12679. doi:10.1016/j.ijhydene.2020.02.126

Bellouard, Q., Abanades, S., and Rodat, S. (2017a). Biomass gasification in an innovative spouted-bed solar reactor: Experimental proof of concept and parametric study. *Energy fuels.* 31 (10), 10933–10945. doi:10.1021/acs.energyfuels.7b01839

Bellouard, Q., Abanades, S., Rodat, S., and Dupassieux, N. (2017b). Solar thermochemical gasification of wood biomass for syngas production in a high-temperature continuously-fed tubular reactor. *Int. J. Hydrogen Energy* 42 (19), 13486–13497. doi:10.1016/j.ijhydene.2016.08.196

Bellouard, Q., Rodat, S., Abanades, S., Ravel, S., and Frayssines, P.-É. (2019). Design, simulation and experimental study of a directly-irradiated solar chemical reactor for hydrogen and syngas production from continuous solar-driven wood biomass gasification. *Int. J. Hydrogen Energy* 44 (35), 19193–19205. doi:10.1016/j.ijhydene.2018.04.147

Boujjat, H., Rodat, S., and Abanades, S. (2020a). Solar-hybrid thermochemical gasification of wood particles and solid recovered fuel in a continuously-fed prototype reactor. *Energies* 13 (19), 5217. doi:10.3390/en13195217

Boujjat, H., Rodat, S., Chuayboon, S., and Abanades, S. (2020b). Experimental and CFD investigation of inert bed materials effects in a high-temperature conical cavity-type reactor for continuous solar-driven steam gasification of biomass. *Chem. Eng. Sci.* 228, 115970. doi:10.1016/j.ces.2020.115970

Boujjat, H., Rodat, S., Chuayboon, S., and Abanades, S. (2019a). Experimental and numerical study of a directly irradiated hybrid solar/combustion spouted bed reactor for continuous steam gasification of biomass. *Energy* 189, 116118. doi:10.1016/j.energy.2019.116118

Boujjat, H., Rodat, S., Chuayboon, S., and Abanades, S. (2019b). Numerical simulation of reactive gas-particle flow in a solar jet spouted bed reactor for continuous biomass gasification. *Int. J. Heat Mass Transf.* 144, 118572. doi:10.1016/j.ijheatmasstransfer.2019.118572

Boujjat, H., Yuki Junior, G. M., Rodat, S., and Abanades, S. (2020c). Dynamic simulation and control of solar biomass gasification for hydrogen-rich syngas production during allothermal and hybrid solar/autothermal operation. *Int. J. Hydrogen Energy* 45 (48), 25827–25837. doi:10.1016/j.ijhydene.2020.01.072

Bruckner, A. P. (1985). Continuous duty solar coal gasification system using molten slag and direct-contact heat exchange. *Sol. Energy* 34 (3), 239–247. doi:10.1016/0038-092X(85)90061-1

Bulfin, B., Miranda, M., and Steinfeld, A. (2021). Performance indicators for benchmarking solar thermochemical fuel processes and reactors. *Front. Energy Res.* 9, 7980. doi:10.3389/fenrg.2021.677980

Cao, L., Yu, I. K. M., Xiong, X., Tsang, D. C. W., Zhang, S., Clark, J. H., et al. (2020). Biorenewable hydrogen production through biomass gasification: A review and future prospects. *Environ. Res.* 186, 109547. doi:10.1016/j.envres.2020.109547

Centi, G., and Perathoner, S. (2010). Towards solar fuels from water and CO2. *Chemsuschem* 3 (2), 195–208. doi:10.1002/cssc.200900289

Chen, J., Lu, Y., Guo, L., Zhang, X., and Xiao, P. (2010). Hydrogen production by biomass gasification in supercritical water using concentrated solar energy: System development and proof of concept. *Int. J. Hydrogen Energy* 35 (13), 7134–7141. doi:10.1016/j.ijhydene.2010.02.023

Chu, S., and Majumdar, A. (2012). Opportunities and challenges for a sustainable energy future. *Nature* 488 (7411), 294–303. doi:10.1038/nature11475

Chuayboon, S., and Abanades, S. (2020). An overview of solar decarbonization processes, reacting oxide materials, and thermochemical reactors for hydrogen and syngas production. *Int. J. Hydrogen Energy* 45 (48), 25783–25810. doi:10.1016/j.ijhydene.2020.04.098

Chuayboon, S., Abanades, S., and Rodat, S. (2018a). Comprehensive performance assessment of a continuous solar-driven biomass gasifier. *Fuel Process. Technol.* 182, 1–14. doi:10.1016/j.fuproc.2018.10.016

Chuayboon, S., Abanades, S., and Rodat, S. (2018b). Experimental analysis of continuous steam gasification of wood biomass for syngas production in a high-temperature particle-fed solar reactor. *Chem. Eng. Process. - Process Intensif.* 125, 253–265. doi:10.1016/j.cep.2018.02.004

Chuayboon, S., Abanades, S., and Rodat, S. (2019). Insights into the influence of biomass feedstock type, particle size and feeding rate on thermochemical performances of a continuous solar gasification reactor. *Renew. Energy* 130, 360–370. doi:10.1016/j.renene.2018.06.065

Curcio, A., Rodat, S., Vuillerme, V., and Abanades, S. (2022). Design and validation of reactant feeding control strategies for the solar-autothermal hybrid gasification of woody biomass. *Energy* 254, 124481. doi:10.1016/j.energy.2022.124481

Curcio, A., Rodat, S., Vuillerme, V., and Abanades, S. (2021). Experimental assessment of woody biomass gasification in a hybridized solar powered reactor featuring direct and indirect heating modes. *Int. J. Hydrogen Energy* 46 (75), 37192–37207. doi:10.1016/j.ijhydene.2021.09.008

Dai, T., Xu, C., Zhang, Q., Liu, X., Chang, Z., and Yang, Y. (2022). Experimental study of the solar-driven steam gasification of coal in an improved updraft combined drop-tube and fixed-bed reactor. *Energy Convers. Manag.* 259, 115571. doi:10.1016/j.enconman.2022.115571

Fang, Y., Paul, M. C., Varjani, S., Li, X., Park, Y.-K., and You, S. (2021). Concentrated solar thermochemical gasification of biomass: Principles, applications, and development. *Renew. Sustain. Energy Rev.* 150, 111484. doi:10.1016/j.rser.2021.111484

Flechsenhar, M., and Sasse, C. (1995). Solar gasification of biomass using oil shale and coal as candidate materials. *Energy* 20 (8), 803–810. doi:10.1016/0360-5442(95)00023-A

Fukuzumi, S. (2017). Production of liquid solar fuels and their use in fuel cells. *Joule* 1 (4), 689–738. doi:10.1016/j.joule.2017.07.007

Gokon, N., Izawa, T., Abe, T., and Kodama, T. (2014). Steam gasification of coal cokes in an internally circulating fluidized bed of thermal storage material for solar thermochemical processes. *Int. J. Hydrogen Energy* 39 (21), 11082–11093. doi:10.1016/j.ijhydene.2014.05.124

Gokon, N., Izawa, T., and Kodama, T. (2015). Steam gasification of coal cokes by internally circulating fluidized-bed reactor by concentrated Xe-light radiation for solar syngas production. *Energy* 79, 264–272. doi:10.1016/j.energy.2014.11.012

Gokon, N., Kumaki, S., Miyaguchi, Y., Bellan, S., Kodama, T., and Cho, H. (2019). Development of a 5kW(th) internally circulating fluidized bed reactor containing quartz sand for continuously-fed coal-coke gasification and a beam-down solar concentrating system. *Energy* 166, 1–16. doi:10.1016/j.energy.2018.10.036

Gokon, N., Ono, R., Hatamachi, T., Li, L., Kim, H.-J., and Kodama, T. (2012). CO2 gasification of coal cokes using internally circulating fluidized bed reactor by concentrated Xe-light irradiation for solar gasification. *Int. J. Hydrogen Energy* 37 (17), 12128–12137. doi:10.1016/j.ijhydene.2012.05.133

Golberg, A., Polikovsky, M., Epstein, M., Slegers, P. M., Drabik, D., and Kribus, A. (2021). Hybrid solar-seaweed biorefinery for co-production of biochemicals, biofuels, electricity, and water: Thermodynamics, life cycle assessment, and cost-benefit analysis. *Energy Convers. Manag.* 246, 114679. doi:10.1016/j.enconman.2021.114679

Gómez-Barea, A., Suárez-Almeida, M., and Ghoniem, A. (2021). Analysis of fluidized bed gasification of biomass assisted by solar-heated particles. *Biomass Convers. biorefin.* 11 (1), 143–158. doi:10.1007/s13399-020-00865-0

Gregg, D. W., Aiman, W. R., Otsuki, H. H., and Thorsness, C. B. (1980a). Solar coal gasification. *Sol. Energy* 24 (3), 313–321. doi:10.1016/0038-092X(80)90489-2

Gregg, D. W., Taylor, R. W., Campbell, J. H., Taylor, J. R., and Cotton, A. (1980b). Solar gasification of coal, activated carbon, coke and coal and biomass mixtures. *Sol. Energy* 25 (4), 353–364. doi:10.1016/0038-092X(80)90347-3

Guo, P., Saw, W. L., van Eyk, P. J., Stechel, E. B., Ashman, P. J., and Nathan, G. J. (2017). System optimization for fischer–tropsch liquid fuels production via solar hybridized dual fluidized bed gasification of solid fuels. *Energy fuels.* 31 (2), 2033–2043. doi:10.1021/acs.energyfuels.6b01755

Guo, P., van Eyk, P. J., Saw, W. L., Ashman, P. J., Nathan, G. J., and Stechel, E. B. (2015). Performance assessment of fischer–tropsch liquid fuels production by solar hybridized dual fluidized bed gasification of lignite. *Energy fuels.* 29 (4), 2738–2751. doi:10.1021/acs.energyfuels.5b00007

Gutiérrez, R. E., Guerra, K., and Haro, P. (2022). Exploring the techno-economic feasibility of new bioeconomy concepts: Solar-assisted thermochemical biorefineries. *Appl. Energy* 322, 119535. doi:10.1016/j.apenergy.2022.119535

Hanchate, N., Ramani, S., Mathpati, C. S., and Dalvi, V. H. (2021). Biomass gasification using dual fluidized bed gasification systems: A review. *J. Clean. Prod.* 280, 123148. doi:10.1016/j.jclepro.2020.123148

Hathaway, B. J., and Davidson, J. H. (2021). Autothermal hybridization and controlled production of hydrogen-rich syngas in a molten salt solar gasifier. *Int. J. Hydrogen Energy* 46 (29), 15257–15267. doi:10.1016/j.ijhydene.2021.02.048

Hathaway, B. J., and Davidson, J. H. (2017). Demonstration of a prototype molten salt solar gasification reactor. *Sol. Energy* 142, 224–230. doi:10.1016/j.solener.2016.12.032

Hathaway, B. J., Davidson, J. H., and Kittelson, D. B. (2011). Solar gasification of biomass: Kinetics of pyrolysis and steam gasification in molten salt. *J. Sol. Energy Eng.* 133 (2), 3680. doi:10.1115/1.4003680

Hathaway, B. J., and Davidson, J. H. (2020). Solar steam gasification of cellulose in a molten alkali salt: Salt chemistry and reactor performance. *Energy fuels.* 34 (2), 1811–1821. doi:10.1021/acs.energyfuels.9b03488

Hathaway, B. J., Honda, M., Kittelson, D. B., and Davidson, J. H. (2013a). Steam gasification of plant biomass using molten carbonate salts. *Energy* 49, 211–217. doi:10.1016/j.energy.2012.11.006

Hathaway, B. J., Kittelson, D. B., and Davidson, J. H. (2013b). Integration of solar gasification with conventional fuel production: The roles of storage and hybridization. *J. Sol. Energy Eng.* 136 (1), 5971. doi:10.1115/1.4025971

He, Y.-L., Qiu, Y., Wang, K., Yuan, F., Wang, W.-Q., Li, M.-J., et al. (2020). Perspective of concentrating solar power. *Energy* 198, 117373. doi:10.1016/j.energy.2020.117373

Heidenreich, S., and Foscolo, P. U. (2015). New concepts in biomass gasification. *Prog. Energy Combust. Sci.* 46, 72–95. doi:10.1016/j.pecs.2014.06.002

Huang, B.-S., Chen, H.-Y., Chuang, K.-H., Yang, R.-X., and Wey, M.-Y. (2012). Hydrogen production by biomass gasification in a fluidized-bed reactor promoted by an Fe/CaO catalyst. *Int. J. Hydrogen Energy* 37 (8), 6511–6518. doi:10.1016/j.ijhydene.2012.01.071

Jie Ling, J. L., Go, E. S., Park, Y.-K., and Lee, S. H. (2022). Recent advances of hybrid solar - biomass thermo-chemical conversion systems. *Chemosphere* 290, 133245. doi:10.1016/j.chemosphere.2021.133245

Kaniyal, A. A., van Eyk, P. J., Nathan, G. J., Ashman, P. J., and Pincus, J. J. (2013b). Polygeneration of liquid fuels and electricity by the atmospheric pressure hybrid solar gasification of coal. *Energy fuels.* 27 (6), 3538–3555. doi:10.1021/ef400198v

Kaniyal, A. A., van Eyk, P. J., and Nathan, G. J. (2013a). Dynamic modeling of the coproduction of liquid fuels and electricity from a hybrid solar gasifier with various fuel blends. *Energy fuels.* 27 (6), 3556–3569. doi:10.1021/ef400217n

Karan, H., Roles, J., Ross, I. L., Ebrahimi, M., Rackemann, D., Rainey, T., et al. (2022). Solar biorefinery concept for sustainable co-production of microalgae-based protein and renewable fuel. *J. Clean. Prod.* 368, 132981. doi:10.1016/j.jclepro.2022.132981

Karl, J., and Proell, T. (2018). Steam gasification of biomass in dual fluidized bed gasifiers: A review. *Renew. Sustain. Energy Rev.* 98, 64–78. doi:10.1016/j.rser.2018.09.010

Kaur, R., Gera, P., Jha, M. K., and Bhaskar, T. (2019). "Chapter 8 - Thermochemical Route for Biohydrogen Production," in *Biohydrogen*. 2nd Edn. Editors A. Pandey, S. V. Mohan, J.-S. Chang, P. C. Hallenbeck, and C. Larroche (Amsterdam: Elsevier), 187–218. doi:10.1016/B978-0-444-64203-5.00008-3

Kodama, T., Gokon, N., Enomoto, S.-i., Itoh, S., and Hatamachi, T. (2010). Coal coke gasification in a windowed solar chemical reactor for beam-down optics. *J. Sol. Energy Eng.* 132 (4), 2081. doi:10.1115/1.4002081

Kodama, T., Kondoh, Y., Tamagawa, T., Funatoh, A., Shimizu, K. I., and Kitayama, Y. (2002). Fluidized bed coal gasification with CO2 under direct irradiation with concentrated visible light. *Energy fuels.* 16 (5), 1264–1270. doi:10.1021/ef020053x

Konarova, M., Aslam, W., and Perkins, G. (2022). "Chapter 3 - Fischer-Tropsch synthesis to hydrocarbon biofuels: Present status and challenges involved," in *Hydrocarbon biorefinery*. Editors S. K. Maity, K. Gayen, and T. K. Bhowmick (Amsterdam: Elsevier), 77. doi:10.1016/B978-0-12-823306-1.00006-6

Kruesi, M., Jovanovic, Z. R., dos Santos, E. C., Yoon, H. C., and Steinfeld, A. (2013). Solar-driven steam-based gasification of sugarcane bagasse in a combined drop-tube and fixed-bed reactor – thermodynamic, kinetic, and experimental analyses. *Biomass Bioenergy* 52, 173–183. doi:10.1016/j.biombioe.2013.03.003

Kruesi, M., Jovanovic, Z. R., and Steinfeld, A. (2014). A two-zone solar-driven gasifier concept: Reactor design and experimental evaluation with bagasse particles. *Fuel* 117, 680–687. doi:10.1016/j.fuel.2013.09.011

Li, L., Coventry, J., Bader, R., Pye, J., and Lipiński, W. (2016). Optics of solar central receiver systems: A review. *Opt. Express* 24 (14), A985–A1007. doi:10.1364/OE.24.00A985

Li, L., Wang, B., Bader, R., Cooper, T., and Lipiński, W. (2021a). "Chapter One - concentrating collector systems for solar thermal and thermochemical applications," in *Advances in chemical engineering*. Editor W. Lipiński (Cambridge: Academic Press). doi:10.1016/bs.ache.2021.10.001

Li, X., Chen, J., Hu, Q., Chu, P., Dai, Y., and Wang, C.-H. (2021b). Solar-driven gasification in an indirectly-irradiated thermochemical reactor with a clapboard-type internally-circulating fluidized bed. *Energy Convers. Manag.* 248, 114795. doi:10.1016/j.enconman.2021.114795

Li, X., Chen, J., Lipiński, W., Dai, Y., and Wang, C.-H. (2020a). A 28 kWe multi-source high-flux solar simulator: Design, characterization, and modeling. *Sol. Energy* 211, 569–583. doi:10.1016/j.solener.2020.09.089

Li, X., Chen, J. L., Sun, X. Y., Zhao, Y., Chong, C., Dai, Y. J., et al. (2021c). Multi-criteria decision making of biomass gasification-based cogeneration systems with heat storage and solid dehumidification of desiccant coated heat exchangers. *Energy* 233, 121122. doi:10.1016/j.energy.2021.121122

Li, X., Dai, Y. J., and Wang, R. Z. (2015). Performance investigation on solar thermal conversion of a conical cavity receiver employing a beam-down solar tower concentrator. *Sol. Energy* 114, 134–151. doi:10.1016/j.solener.2015.01.033

Li, X., Lin, M., Dai, Y., and Wang, C.-H. (2017). Comparison-based optical assessment of hyperboloid and ellipsoid reflectors in a beam-down solar tower system with linear fresnel heliostats. *J. Sol. Energy Eng.* 139 (6). doi:10.1115/1.4037742

Li, X., Shen, Y., Kan, X., Hardiman, T. K., Dai, Y., and Wang, C.-H. (2018). Thermodynamic assessment of a solar/autothermal hybrid gasification CCHP system with an indirectly radiative reactor. *Energy* 142, 201–214. doi:10.1016/j.energy.2017.09.149

Li, X., Shen, Y., Wei, L., He, C., Lapkin, A. A., Lipiński, W., et al. (2020b). Hydrogen production of solar-driven steam gasification of sewage sludge in an indirectly irradiated fluidized-bed reactor. *Appl. Energy* 261, 114229. doi:10.1016/j.apenergy.2019.114229

Li, X., and Wang, C.-H. (2020). 2017 P.V. Danckwerts Memorial Lecture special issue editorial: Advances in emerging technologies of chemical engineering towards sustainable energy and environment: Solar and biomass. *Chem. Eng. Sci.* 215, 115384. doi:10.1016/j.ces.2019.115384

Li, Z., Lin, Q., Li, M., Cao, J., Liu, F., Pan, H., et al. (2020c). Recent advances in process and catalyst for CO2 reforming of methane. *Renew. Sustain. Energy Rev.* 134, 110312. doi:10.1016/j.rser.2020.110312

Liao, B., Guo, L., Lu, Y., and Zhang, X. (2013). Solar receiver/reactor for hydrogen production with biomass gasification in supercritical water. *Int. J. Hydrogen Energy* 38 (29), 13038–13044. doi:10.1016/j.ijhydene.2013.03.113

Lichty, P., Perkins, C., Woodruff, B., Bingham, C., and Weimer, A. (2010). Rapid high temperature solar thermal biomass gasification in a prototype cavity reactor. *J. Sol. Energy Eng.* 132 (1), 356. doi:10.1115/1.4000356

Lipiński, W., Abbasi-Shavazi, E., Chen, J., Coventry, J., Hangi, M., Iyer, S., et al. (2021). Progress in heat transfer research for high-temperature solar thermal applications. *Appl. Therm. Eng.* 184, 116137. doi:10.1016/j.applthermaleng.2020.116137

Liu, Q., Bai, Z., Wang, X., Lei, J., and Jin, H. (2016). Investigation of thermodynamic performances for two solar-biomass hybrid combined cycle power generation systems. *Energy Convers. Manag.* 122, 252–262. doi:10.1016/j.enconman.2016.05.080

Liu, R., Liu, M., Zhao, Y., Ma, Y., and Yan, J. (2021). Thermodynamic study of a novel lignite poly-generation system driven by solar energy. *Energy* 214, 119075. doi:10.1016/j.energy.2020.119075

Loutzenhiser, P. G., and Muroyama, A. P. (2017). A review of the state-of-the-art in solar-driven gasification processes with carbonaceous materials. *Sol. Energy* 156, 93–100. doi:10.1016/j.solener.2017.05.008

Lu, Y., Zhao, L., and Guo, L. (2011). Technical and economic evaluation of solar hydrogen production by supercritical water gasification of biomass in China. *Int. J. Hydrogen Energy* 36 (22), 14349–14359. doi:10.1016/j.ijhydene.2011.07.138

Maag, G., and Steinfeld, A. (2010). Design of a 10 MW particle-flow reactor for syngas production by steam-gasification of carbonaceous feedstock using concentrated solar energy. *Energy fuels.* 24 (12), 6540–6547. doi:10.1021/ef100936j

Matsunami, J., Yoshida, S., Oku, Y., Yokota, O., Tamaura, Y., and Kitamura, M. (2000). Coal gasification by CO2 gas bubbling in molten salt for solar/fossil energy hybridization. *Sol. Energy* 68 (3), 257–261. doi:10.1016/S0038-092X(99)00074-2

Melchior, T., Perkins, C., Lichty, P., Weimer, A. W., and Steinfeld, A. (2009). Solar-driven biochar gasification in a particle-flow reactor. *Chem. Eng. Process. Process Intensif.* 48 (8), 1279–1287. doi:10.1016/j.cep.2009.05.006

Möller, S. (2008). "Solref - solar steam reforming of methane rich gas for synthesis gas production," in *Deutsches Zentrum für Luft- und Raumfahrt e.V.* Editor M. Geyer.

Müller, F., Patel, H., Blumenthal, D., Poživil, P., Das, P., Wieckert, C., et al. (2018). Co-production of syngas and potassium-based fertilizer by solar-driven thermochemical conversion of crop residues. *Fuel Process. Technol.* 171, 89–99. doi:10.1016/j.fuproc.2017.08.006

Müller, F., Poživil, P., van Eyk, P. J., Villarrazo, A., Haueter, P., Wieckert, C., et al. (2017). A pressurized high-flux solar reactor for the efficient thermochemical gasification of carbonaceous feedstock. *Fuel* 193, 432–443. doi:10.1016/j.fuel.2016.12.036

Müller, R., Zedtwitz, P. v., Wokaun, A., and Steinfeld, A. (2003). Kinetic investigation on steam gasification of charcoal under direct high-flux irradiation. *Chem. Eng. Sci.* 58 (22), 5111–5119. doi:10.1016/j.ces.2003.08.018

Muroyama, A. P., Guscetti, I., Schieber, G. L., Haussener, S., and Loutzenhiser, P. G. (2018). Design and demonstration of a prototype 1.5kWth hybrid solar/autothermal steam gasifier. *Fuel* 211, 331–340. doi:10.1016/j.fuel.2017.09.059

Muroyama, A., Shinn, T., Fales, R., and Loutzenhiser, P. G. (2014). Modeling of a dynamically-controlled hybrid solar/autothermal steam gasification reactor. *Energy fuels.* 28 (10), 6520–6530. doi:10.1021/ef501535r

Murray, J. P., and Fletcher, E. A. (1994). Reaction of steam with cellulose in a fluidized bed using concentrated sunlight. *Energy* 19 (10), 1083–1098. doi:10.1016/0360-5442(94)90097-3

Nzihou, A., Flamant, G., and Stanmore, B. (2012). Synthetic fuels from biomass using concentrated solar energy – a review. *Energy* 42 (1), 121–131. doi:10.1016/j.energy.2012.03.077

Pfahl, A., Coventry, J., Röger, M., Wolfertstetter, F., Vásquez-Arango, J. F., Gross, F., et al. (2017). Progress in heliostat development. *Sol. Energy* 152, 3–37. doi:10.1016/j.solener.2017.03.029

Piatkowski, N., and Steinfeld, A. (2008). Solar-driven coal gasification in a thermally irradiated packed-bed reactor. *Energy fuels.* 22 (3), 2043–2052. doi:10.1021/ef800027c

Piatkowski, N., Wieckert, C., and Steinfeld, A. (2009). Experimental investigation of a packed-bed solar reactor for the steam-gasification of carbonaceous feedstocks. *Fuel Process. Technol.* 90 (3), 360–366. doi:10.1016/j.fuproc.2008.10.007

Piatkowski, N., Wieckert, C., Weimer, A. W., and Steinfeld, A. (2011). Solar-driven gasification of carbonaceous feedstock—A review. *Energy Environ. Sci.* 4 (1), 73–82. doi:10.1039/C0EE00312C

Puig-Arnavat, M., Tora, E. A., Bruno, J. C., and Coronas, A. (2013). State of the art on reactor designs for solar gasification of carbonaceous feedstock. *Sol. Energy* 97, 67–84. doi:10.1016/j.solener.2013.08.001

Rabl, A. (1976). Tower reflector for solar power plant. *Sol. Energy* 18 (3), 269–271. doi:10.1016/0038-092X(76)90027-X

Rahbari, A., Shirazi, A., Venkataraman, M. B., and Pye, J. (2019). A solar fuel plant via supercritical water gasification integrated with Fischer–Tropsch synthesis: Steady-state modelling and techno-economic assessment. *Energy Convers. Manag.* 184, 636–648. doi:10.1016/j.enconman.2019.01.033

Rahbari, A., Shirazi, A., Venkataraman, M. B., and Pye, J. (2021). Solar fuels from supercritical water gasification of algae: Impacts of low-cost hydrogen on reformer configurations. *Appl. Energy* 288, 116620. doi:10.1016/j.apenergy.2021.116620

Rinaldi, F., Binotti, M., Giostri, A., and Manzolini, G. (2014). Comparison of linear and point focus collectors in solar power plants. *Energy Procedia* 49, 1491–1500. doi:10.1016/j.egypro.2014.03.158

Roeb, M., Säck, J. P., Rietbrock, P., Prahl, C., Schreiber, H., Neises, M., et al. (2011). Test operation of a 100kW pilot plant for solar hydrogen production from water on a solar tower. *Sol. Energy* 85 (4), 634–644. doi:10.1016/j.solener.2010.04.014

Romero, M., and Steinfeld, A. (2012). Concentrating solar thermal power and thermochemical fuels. *Energy Environ. Sci.* 5 (11), 9234–9245. doi:10.1039/C2EE21275G

Roy, S. C., Varghese, O. K., Paulose, M., and Grimes, C. A. (2010). Toward solar fuels: Photocatalytic conversion of carbon dioxide to hydrocarbons. *Acs Nano* 4 (3), 1259–1278. doi:10.1021/nn9015423

Schappi, R., Rutz, D., Daehler, F., Muroyama, A., Haueter, P., Lilliestam, J., et al. (2021). Drop-in fuels from sunlight and air. *Nature*, 63, 63. doi:10.1038/s41586-021-04174-y

Service, R. F. (2009). Biomass fuel starts to see the light. *Science* 326, 1474. doi:10.1126/science.326.5959.1474

Shih, C. F., Zhang, T., Li, J. H., and Bai, C. L. (2018). Powering the future with liquid sunshine. *Joule* 2 (10), 1925–1949. doi:10.1016/j.joule.2018.08.016

Shirazi, A., Rahbari, A., Asselineau, C.-A., and Pye, J. (2019). A solar fuel plant via supercritical water gasification integrated with Fischer–Tropsch synthesis: System-level dynamic simulation and optimisation. *Energy Convers. Manag.* 192, 71–87. doi:10.1016/j.enconman.2019.04.008

Steinfeld, A. (2005). Solar thermochemical production of hydrogen–a review. *Sol. Energy* 78 (5), 603–615. doi:10.1016/j.solener.2003.12.012

Suárez-Almeida, M., Gómez-Barea, A., Ghoniem, A. F., and Pfeifer, C. (2021). Solar gasification of biomass in a dual fluidized bed. *Chem. Eng. J.* 406, 126665. doi:10.1016/j.cej.2020.126665

Tanger, P., Field, J., Jahn, C., DeFoort, M., and Leach, J. (2013). Biomass for thermochemical conversion: Targets and challenges. *Front. Plant Sci.* 4, 218. doi:10.3389/fpls.2013.00218

Taylor, R. W., Berjoan, R., and Coutures, J. P. (1983). Solar gasification of carbonaceous materials. *Sol. Energy* 30 (6), 513–525. doi:10.1016/0038-092X(83)90063-4

Tregambi, C., Troiano, M., Montagnaro, F., Solimene, R., and Salatino, P. (2021). Fluidized beds for concentrated solar thermal technologies—a review. *Front. Energy Res.* 9, 8421. doi:10.3389/fenrg.2021.618421

Troiano, M., Chinnici, A., Bellan, S., and Nathan, G. J. (2022). Editorial: Technological and fundamental advances in production, storage and utilization of fuels. *Front. Energy Res.* 10, 772. doi:10.3389/fenrg.2022.830772

van Eyk, P. J., Ashman, P. J., and Nathan, G. J. (2016). Effect of high-flux solar irradiation on the gasification of coal in a hybrid entrained-flow reactor. *Energy fuels.* 30 (6), 5138–5147. doi:10.1021/acs.energyfuels.6b00342

Vant-Hull, L. (2014). Issues with beam-down concepts. *Energy Procedia* 49, 257–264. doi:10.1016/j.egypro.2014.03.028

Villafán-Vidales, H. I., Arancibia-Bulnes, C. A., Riveros-Rosas, D., Romero-Paredes, H., and Estrada, C. A. (2017). An overview of the solar thermochemical processes for hydrogen and syngas production: Reactors, and facilities. *Renew. Sustain. Energy Rev.* 75, 894–908. doi:10.1016/j.rser.2016.11.070

von Zedtwitz, P., Lipiński, W., and Steinfeld, A. (2007). Numerical and experimental study of gas–particle radiative heat exchange in a fluidized-bed reactor for steam-gasification of coal. *Chem. Eng. Sci.* 62 (1), 599–607. doi:10.1016/j.ces.2006.09.027

von Zedtwitz, P., and Steinfeld, A. (2005). Steam-gasification of coal in a fluidized-bed/packed-bed reactor exposed to concentrated thermal RadiationModeling and experimental validation. *Ind. Eng. Chem. Res.* 44 (11), 3852–3861. doi:10.1021/ie050138w

Wang, B., Li, X., Dai, Y., and Wang, C.-H. (2022). Thermodynamic analysis of an epitrochoidal rotary reactor for solar hydrogen production via a water-splitting thermochemical cycle using nonstoichiometric ceria. *Energy Convers. Manag.* 268, 115968. doi:10.1016/j.enconman.2022.115968

Wang, J., Ma, C., and Wu, J. (2019). Thermodynamic analysis of a combined cooling, heating and power system based on solar thermal biomass gasification. *Appl. Energy* 247, 102. doi:10.1016/j.apenergy.2019.04.039

Wang, S., Dai, G., Yang, H., and Luo, Z. (2017). Lignocellulosic biomass pyrolysis mechanism: A state-of-the-art review. *Prog. Energy Combust. Sci.* 62, 33–86. doi:10.1016/j.pecs.2017.05.004

Weinstein, L. A., Loomis, J., Bhatia, B., Bierman, D. M., Wang, E. N., and Chen, G. (2015). Concentrating solar power. *Chem. Rev.* 115 (23), 12797–12838. doi:10.1021/acs.chemrev.5b00397

Wieckert, C., Frommherz, U., Kräupl, S., Guillot, E., Olalde, G., Epstein, M., et al. (2006). A 300kW solar chemical pilot plant for the carbothermic production of zinc. *J. Sol. Energy Eng.* 129 (2), 190–196. doi:10.1115/1.2711471

Wieckert, C., Obrist, A., Zedtwitz, P. v., Maag, G., and Steinfeld, A. (2013). Syngas production by thermochemical gasification of carbonaceous waste materials in a 150 kWth packed-bed solar reactor. *Energy fuels.* 27 (8), 4770–4776. doi:10.1021/ef4008399

Wörner, A., and Tamme, R. (1998). CO2 reforming of methane in a solar driven volumetric receiver–reactor. *Catal. Today* 46 (2), 165–174. doi:10.1016/S0920-5861(98)00338-1

Wu, H., Liu, Q., Bai, Z., Xie, G., and Zheng, J. (2019). Performance investigation of a novel multi-functional system for power, heating and hydrogen with solar energy and biomass. *Energy Convers. Manag.* 196, 768–778. doi:10.1016/j.enconman.2019.06.040

Wu, H., Liu, Q., Bai, Z., Xie, G., Zheng, J., and Su, B. (2020). Thermodynamics analysis of a novel steam/air biomass gasification combined cooling, heating and power system with solar energy. *Appl. Therm. Eng.* 164, 114494. doi:10.1016/j.applthermaleng.2019.114494

Xiao, P., Guo, L., Zhang, X., Zhu, C., and Ma, S. (2013). Continuous hydrogen production by biomass gasification in supercritical water heated by molten salt flow: System development and reactor assessment. *Int. J. Hydrogen Energy* 38 (29), 12927–12937. doi:10.1016/j.ijhydene.2013.04.139

Xin, T., Xu, C., Liu, Y., and Yang, Y. (2022). Thermodynamic analysis and economic evaluation of a novel coal-based zero emission polygeneration system using solar gasification. *Appl. Therm. Eng.* 201, 117814. doi:10.1016/j.applthermaleng.2021.117814

Xu, C., Xin, T., Li, X., Li, S., Sun, Y., Liu, W., et al. (2019). A thermodynamic analysis of a solar hybrid coal-based direct-fired supercritical carbon dioxide power cycle. *Energy Convers. Manag.* 196, 77–91. doi:10.1016/j.enconman.2019.06.002

Xue, Y., Zhou, S., Brown, R. C., Kelkar, A., and Bai, X. (2015). Fast pyrolysis of biomass and waste plastic in a fluidized bed reactor. *Fuel* 156, 40–46. doi:10.1016/j.fuel.2015.04.033

Yogev, A., Kribus, A., Epstein, M., and Kogan, A. (1998). Solar "tower reflector" systems: A new approach for high-temperature solar plants. *Int. J. Hydrogen Energy* 23 (4), 239–245. doi:10.1016/s0360-3199(97)00059-1

Yoon, H. C., Cooper, T., and Steinfeld, A. (2011). Non-catalytic autothermal gasification of woody biomass. *Int. J. Hydrogen Energy* 36 (13), 7852–7860. doi:10.1016/j.ijhydene.2011.01.138

Z'Graggen, A., and Steinfeld, A. (2008). Hydrogen production by steam-gasification of carbonaceous materials using concentrated solar energy – V. Reactor modeling, optimization, and scale-up. *Int. J. Hydrogen Energy* 33 (20), 5484–5492. doi:10.1016/j.ijhydene.2008.07.047

Z'Graggen, A., Haueter, P., Maag, G., Romero, M., and Steinfeld, A. (2008). Hydrogen production by steam-gasification of carbonaceous materials using concentrated solar energy—IV. Reactor experimentation with vacuum residue. *Int. J. Hydrogen Energy* 33 (2), 679–684. doi:10.1016/j.ijhydene.2007.10.038

Z'Graggen, A., Haueter, P., Maag, G., Vidal, A., Romero, M., and Steinfeld, A. (2007). Hydrogen production by steam-gasification of petroleum coke using concentrated solar power—III. Reactor experimentation with slurry feeding. *Int. J. Hydrogen Energy* 32 (8), 992–996. doi:10.1016/j.ijhydene.2006.10.001

Z'Graggen, A., Haueter, P., Trommer, D., Romero, M., de Jesus, J. C., and Steinfeld, A. (2006). Hydrogen production by steam-gasification of petroleum coke using concentrated solar power—II reactor design, testing, and modeling. *Int. J. Hydrogen Energy* 31 (6), 797–811. doi:10.1016/j.ijhydene.2005.06.011

Zhong, D., Zeng, K., Li, J., Yang, X., Song, Y., Zhu, Y., et al. (2021). 3E analysis of a biomass-to-liquids production system based on solar gasification. *Energy* 217, 119408. doi:10.1016/j.energy.2020.119408

Zhou, X., Li, W., Mabon, R., and Broadbelt, L. J. (2018). A mechanistic model of fast pyrolysis of hemicellulose. *Energy Environ. Sci.* 11 (5), 1240–1260. doi:10.1039/c7ee03208k

Nomenclature

Symbols

$\boldsymbol{A_{conc}}$ Aperture area of the concentrator

$\boldsymbol{A_{rec}}$ Aperture area of the receiver

$\boldsymbol{C_f}$ Flux concentration ratio

$\boldsymbol{C_g}$ Geometrical concentration ratio

ϕ Equivalence ratio

ΔH_i Standard enthalpy of reaction i

η_{abs} Absorption efficiency

η_{opt} Optical efficiency

$\eta_{solar-to-chemical}$ Solar-to-chemical efficiency

$\eta_{solar-to-fuel}$ Solar-to-fuel energy conversion efficiency

$\boldsymbol{LHV_i}$ Lower heating value of species i

$\boldsymbol{m_i}$ Mass of species i

$\boldsymbol{n_i}$ Number of moles of species i

σ Stefan-Boltzmann constant

$\dot{Q}_{rec}$ Power collected by the receiver aperture

$\boldsymbol{Q_{solar}}$ Solar energy input

θ_{sun} Divergence half-angle of sunlight on Earth

$\boldsymbol{T_{rec}}$ Temperature of receiver

$\boldsymbol{U}$ Energy upgrade factor

$\boldsymbol{X_C}$ Carbon conversion rate

ψ_{rim} Rim angle of the concentrator

Abbreviations

CCHP Combined cooling heat and power

CR Central receiver

CSP Concentrating solar power

CSTGB Concentrated solar thermochemical gasification of biomass

DEAC Double-effect absorption chiller

DFB Dual fluidized bed

DHX Droplet heat exchanger

DME Dimethyl ether

DNI Direct normal incident solar radiation

FT Fischer-Tropsch

FTS Fischer-Tropsch synthesis

HTF Heat transfer fluid

ICE Internal combustion engine

ICFB Internally circulating fluidized bed

LCOF Levelized cost of fuel

SAHG Solar/autothermal hybrid gasification

SCW Supercritical water

SCWG Solar-driven supercritical water gasification

SDFB Solar hybrid dual fluidized bed

SGCC Solar gasification combined cycle

SHCC Solar hybrid combined cycle

WGS Water-gas shift

WGSR Water-gas shift reaction